

# Coupled charge and energy transfer dynamics in light harvesting complexes from a hybrid hierarchical equations of motion approach

Thomas P. Fay<sup>1, a)</sup> and David T. Limmer<sup>1, 2, 3, 4, b)</sup>

<sup>1)</sup>*Department of Chemistry, University of California, Berkeley, CA 94720, USA*

<sup>2)</sup>*Kavli Energy Nanoscience Institute at Berkeley, Berkeley, CA 94720, USA*

<sup>3)</sup>*Chemical Sciences Division, Lawrence Berkeley National Laboratory, Berkeley, CA 94720, USA*

<sup>4)</sup>*Materials Science Division, Lawrence Berkeley National Laboratory, Berkeley, CA 94720, USA*

We describe a method for simulating exciton dynamics in protein-pigment complexes, including effects from charge transfer as well as fluorescence. The method combines the hierarchical equations of motion, which are used to describe quantum dynamics of excitons, and the Nakajima-Zwanzig quantum master equation, which is used to describe slower charge transfer processes. We study the charge transfer quenching in light harvesting complex II, a protein postulated to control non-photochemical quenching in many plant species. Using our hybrid approach, we find good agreement between our calculation and experimental measurements of the excitation lifetime. Furthermore our calculations reveal that the exciton energy funnel plays an important role in determining quenching efficiency, a conclusion we expect to extend to other proteins that perform protective excitation quenching. This also highlights the need for simulation methods that properly account for the interplay of exciton dynamics and charge transfer processes.

## I. INTRODUCTION

Photosynthetic systems rely on both electronic excitation energy transfer and charge transfer processes to perform the reactions that sustain life on Earth.<sup>1–5</sup> For example, excitation energy transfer (EET) and charge transfer (CT) play fundamental roles in reaction centers,<sup>4</sup> where light energy from the Sun is harvested to drive chemical reactions. Charge transfer is also likely have an important photo-protective function in photosynthetic organisms,<sup>6–10</sup> by quenching excess excitation energy and preventing damage to photosynthetic systems. The importance of coupled charge and excitation energy transfer dynamics necessitates the development of theoretical methods to accurately and efficiently simulate them together. Here we develop a theory to study both processes using a hybrid approach that combines the hierarchical equation equations (HEOM) with quantum master equations (QME) to afford a computationally efficient method that is also accurate.

Rapid excitation energy transfer has been studied extensively using a variety of methods, with HEOM emerging as a flexible and highly accurate approach for a large class of systems.<sup>11–13</sup> The HEOM method has enabled the simulation of EET in photosynthetic complexes without invoking perturbation theory, enabling a balanced description of both incoherent Förster EET, and coherent excitonic EET, as well as transport dynamics intermediate between these two regimes.<sup>14</sup> Although the HEOM method has been used extensively to study EET,<sup>12,15–25</sup> it has been used less in the study of combined EET and CT.<sup>26</sup> This is largely because charge transfer states typically couple much more strongly to the environment than local electronic excitations. Typical reorganization energies for CT processes are often in excess of  $20k_B T$  at room temperature in polar environments, due to the large changes in charge density distributions on molecules involved in CT,<sup>27</sup> compared to  $\sim 1k_B T$  for chlorophyll excitations. As a result of the large system-

bath coupling strength, direct HEOM calculations involving CT states become very challenging.<sup>28–30</sup> Recent developments using matrix product states,<sup>31–33</sup> and their generalizations,<sup>34</sup> or tree tensor networks<sup>35</sup> to solve the HEOM can help alleviate this problem, but these methods are limited to linear coupling models between the charge transfer states and harmonic environments. Alternative numerically exact methods such as MACGIC-QUAPI<sup>36,37</sup> have been successfully applied to models of coupled EET and CT in reaction centers,<sup>37</sup> but dynamics with this method can still be difficult to converge for large system sizes and strong system-bath coupling. Approximate theories, namely modified-Redfield/generalized Förster theory<sup>38–40</sup> have been applied to study CT processes in light-harvesting complexes,<sup>26,41,42</sup> but these methods do not always accurately describe the EET dynamics in the absence of CT processes.<sup>21</sup> Semi-classical approaches have also been used to study exciton dynamics,<sup>43–49</sup> but these methods often break down for systems with large system-bath couplings, as is encountered in CT processes. In order to facilitate the study of reaction center and CT quenching processes in photosynthesis an accurate and computationally efficient method that can describe coupled EET and CT processes is needed.

In this work we present a theory combining the HEOM method, which is used to model the EET dynamics of locally excited states, with quantum master equation approaches used to describe the charge transfer<sup>50–53</sup> and radiative processes.<sup>19</sup> Conceptually similar hybrid approaches in which different degrees of freedom are treated with different levels of theory have been used previously to extend the applicability of approximate theories,<sup>54–57</sup> but here we take the numerically exact HEOM method and make it more computationally tractable through judicious approximations on a subset of dynamical degrees of freedom. The working equations of our method, obtained using a Zwanzig projection approach,<sup>58–60</sup> are a set of simple linear differential equations for hierarchies of auxiliary density operators for the different manifolds of states in the system. Formally the method can account for anharmonicity in the degrees of freedom coupled to the CT processes, though in this work we only consider linear response models for the CT pro-

<sup>a)</sup>Electronic mail: [tom.patrick.fay@gmail.com](mailto:tom.patrick.fay@gmail.com)

<sup>b)</sup>Electronic mail: [dlimmer@berkeley.edu](mailto:dlimmer@berkeley.edu)

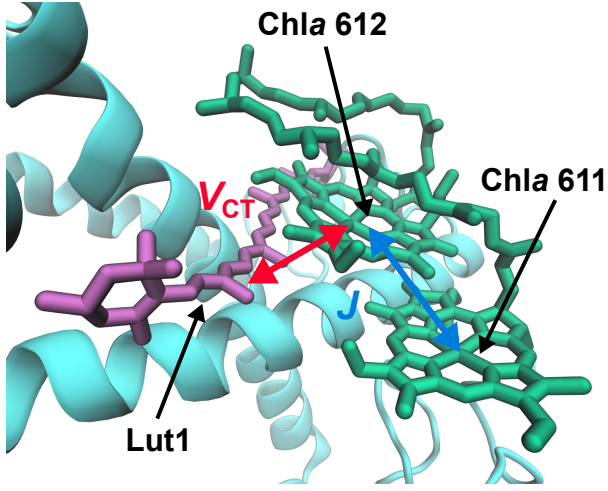


FIG. 1. The structure of the Chla611-Chla612 dimer in LHCII with the lutein (Lut 620) electron donor (PDB 1RWT, chain C<sup>63</sup>). The electron transfer coupling is denoted  $V_{CT}$  and the electrostatic interchromophore coupling is denoted  $J$ .

cess. In Sec. II we outline the model and the HEOM method, and in Sec. III we derive the hybrid HEOM/QME method. In Sec. IV we test the method against exact results for a dimer of locally excited states coupled to a CT state in order to verify the accuracy of the method. In Sec. V we then apply the hybrid HEOM/QME method to study charge transfer quenching in light-harvesting complex II (LHCII),<sup>1,21,40,61,62</sup> a system which would be intractable to study with direct HEOM calculations. Our simulations of LHCII reveal the importance of the excitation energy funnel in determining photo-protective quenching efficiency in the LHCII complex, a result which we discuss further in Sec. VI. Finally we draw conclusions in Sec. VII.

## II. THEORY

We consider the coupled energy and charge transfer of a photoexcited chromophoric system, like that found in naturally occurring light harvesting complexes. In this section, we outline a general model hamiltonian, and review HEOM.

### A. Exciton and charge transfer model

The system we consider consists of chromophores, and electron donors and acceptors. The chromophores have a ground state  $|GS\rangle$ , and a manifold of singly excited states, which can be spanned by a local basis  $|LE_n\rangle$ , which are coupled electrostatically. Such a system of coupled LE states can be well described by a Frenkel exciton model.<sup>1</sup> These locally excited states can also undergo charge transfer, where either the excited electron or hole transfers to a nearby acceptor or donor. The charge transfer states that can be formed by these processes are denoted as  $|CT_n\rangle$ . These states can undergo charge recombination to return the system to  $|GS\rangle$ . An example of such

a system is the Chla 611–Chla 612 dimer in LHCII shown in Fig. 1,<sup>62</sup> where the locally excited Chla states couple to each other, and the locally excited Chla 612 can also accept an electron from the nearby lutein donor. As well as coupling to each other, the LE and CT electronic excitations couple to the nuclear degrees of freedom on the chromophores, the donors/acceptors, and the surrounding polarizable environment, which leads to decoherence and relaxation of these excited electronic states. For example in the Chla dimer in Fig. 1 the local excitation on each Chla couples primarily to the vibrations localized on each chlorophyll,<sup>1</sup> but the CT excitation couples to the intramolecular Chla and lutein vibrations, and the low frequency modes which determine polarization of the surrounding protein and solvent environment.<sup>27</sup> Furthermore the electronic states of the system couple to the electromagnetic field, which creates radiative decay pathways for the excited electronic states.<sup>19</sup>

The Hamiltonian for the system described above can be written as

$$\hat{H} = \hat{H}_{LE} + \hat{H}_{CT} + \hat{H}_{GS} + \hat{H}_{LE,CT} + \hat{H}_{CT,GS} + \hat{H}_{EM} + \hat{H}_D \quad (1)$$

where the ground state Hamiltonian  $\hat{H}_{GS}$  decomposes as

$$\hat{H}_{GS} = \hat{\Pi}_{GS}(\hat{T} + \hat{V}_0), \quad (2)$$

here  $\hat{T}$  is the nuclear kinetic energy operator,  $\hat{V}_0$  is the ground-state potential energy operator, and  $\hat{\Pi}_{GS}$  is a projection operator  $\hat{\Pi}_{GS} = |GS\rangle\langle GS|$ . Similarly the Hamiltonian of the charge transfer states is

$$\hat{H}_{CT} = \sum_{n=1}^{N_{CT}} \hat{\Pi}_{CT_n} \hat{H}_{CT_n} = \sum_{n=1}^{N_{CT}} \hat{\Pi}_{CT_n} (\hat{T} + \hat{V}_{CT_n}) \quad (3)$$

with  $\hat{\Pi}_{CT_n} = |CT_n\rangle\langle CT_n|$  being a projection operator onto the  $CT_n$  state, which we assume is a CT state in which electrons and holes are localized on specific acceptors and donors. For the locally excited states we take a similar form but include all the LE state couplings  $J_{nm}$ ,

$$\begin{aligned} \hat{H}_{LE} = & \left( \sum_{n=1}^{N_{LE}} |LE_n\rangle\langle LE_n| (E_n + \hat{T} + \hat{V}_{LE_n}) \right. \\ & \left. + \sum_{n>m} J_{nm} (|LE_n\rangle\langle LE_m| + |LE_m\rangle\langle LE_n|) \right), \end{aligned} \quad (4)$$

$$= \hat{H}_{LE,s} + \sum_{n=1}^{N_{LE}} |LE_n\rangle\langle LE_n| (\hat{T} + \hat{V}_{LE_n}) \quad (5)$$

and we can again define an electronic projection operator  $\hat{\Pi}_{LE} = \sum_n |LE_n\rangle\langle LE_n|$  which commutes with  $\hat{H}_{LE}$ . The CT-GS diabatic coupling term can be written as

$$\hat{H}_{CT,GS} = \sum_{n=1}^{N_{CT}} V_{CT_n,GS} (|CT_n\rangle\langle GS| + |GS\rangle\langle CT_n|) \quad (6)$$

and the locally excited state charge transfer diabatic coupling term can be written as

$$\hat{H}_{LE,CT} = \sum_{n=1}^{N_{LE}} \sum_{m=1}^{N_{CT}} V_{LE_n,CT_m} (|LE_n\rangle\langle CT_m| + |CT_m\rangle\langle LE_n|). \quad (7)$$

with coupling constants  $V_{CT_n,GS}$  and  $V_{LE_n,CT_m}$ . For simplicity, we have made the Condon approximation, by assuming the diabatic state couplings have no nuclear coordinate dependence.

The electromagnetic field Hamiltonian  $\hat{H}_{EM}$  is given by<sup>19,24</sup>

$$\hat{H}_{EM} = \sum_{k,p} \hbar\omega_k \left( \hat{a}_{kp}^\dagger \hat{a}_{kp} + \frac{1}{2} \right) \quad (8)$$

where  $\hat{a}_{kp}$  is the electromagnetic (EM) field annihilation operator for mode  $k$  with polarization  $p$ , and  $\omega_k = c_0|k|$ . These EM field modes are denoted the  $b_{EM}$  degrees of freedom.  $\hat{H}_D$  is the dipole coupling operator between the molecular system and the EM field,<sup>19,24,64</sup>

$$\hat{H}_D = -\hat{\mu} \cdot \hat{\mathcal{E}} \quad (9)$$

within a point dipole approximation for the system. Here  $\hat{\mu}$  is the system transition dipole moment operator, with components for the  $LE_n$  state,  $\hat{\mu}_{n,\alpha}$ , with  $\alpha = x, y, z$ , given by

$$\hat{\mu}_\alpha = \sum_{n=1}^{N_{LE}} \mu_{n,\alpha} (|LE_n\rangle\langle GS| + |GS\rangle\langle LE_n|), \quad (10)$$

and  $\hat{\mathcal{E}}$  is the electric field operator at the origin,

$$\hat{\mathcal{E}} = i \sum_{k,p} \sqrt{\frac{\hbar\omega_k}{2\mathcal{V}_0\epsilon_0}} \left( \hat{a}_{kp} \mathbf{e}_{kp} - \hat{a}_{kp}^\dagger \mathbf{e}_{kp}^* \right), \quad (11)$$

in which  $\mathcal{V}_0$  is the volume of the system,  $\epsilon_0$  is vacuum permittivity, and  $\mathbf{e}_{kp}$  is a unit vector defining the polarization of the EM field mode  $kp$ .

In describing the potential energy surfaces for the different diabatic states, we start by separating out the nuclear bath coordinates that modulate the energy gap between the  $LE_n$  state and the ground-state, which we denote the  $b_{LE_n}$  degrees of freedom. This is justified by noting that the main degrees of freedom that modulate the  $LE_n$  energies are intramolecular vibrational modes on chromophore  $n$  and its surrounding local environment. Given the  $CT_n$  states involve these chromophores, the  $CT_n$  energies can also depend on the  $b_{LE_n}$  degrees of freedom, as well as local modes on donors/acceptors involved in the charge transfer, and delocalized modes corresponding to environment polarization.<sup>1,12</sup> These additional bath degrees of freedom are denoted  $b_{CT}$ . In what follows we assume that the  $b_{LE}$  and  $b_{CT}$  degrees of freedom are not coupled and are therefore uncorrelated, and operators on these degrees of freedom, indicated by superscript  $b_{LE}$  and  $b_{CT}$  labels, therefore commute. This assumption is analogous to separating intramolecular and environmental contributions to spectral densities used in modeling condensed phase optical spectra,<sup>65–67</sup> and the separation of inner and outer-sphere contributions to electron transfer reorganization energies.<sup>27,30</sup>

Within this assumption, we can write down a model Hamil-

tonian for the coupled LE and CT states as

$$\begin{aligned} \hat{H} = & \hat{H}_{LE,s} + \sum_{n=1}^{N_{LE}} |LE_n\rangle\langle LE_n| \Delta\hat{V}_{LE_n}^{b_{LE_n}} \\ & + \sum_{n=1}^{N_{CT}} \hat{\Pi}_{CT_n} \left( \hat{H}_{CT_n,s} + \Delta\hat{V}_{CT_n}^{b_{CT_n}} + \sum_{m=1}^{N_{LE}} \Delta\hat{V}_{CT_n}^{b_{LE_m}} \right) \\ & + \hat{H}_{GS}^{b_{LE}} + \hat{H}_{GS}^{b_{CT}} + \hat{H}_{ET} + \hat{H}_{EM} + \hat{H}_D. \end{aligned} \quad (12)$$

Here  $\hat{H}_{LE,s}$  is the LE system Hamiltonian, containing the LE state energies and couplings, and similarly  $\hat{H}_{CT_n,s}$  is the system Hamiltonian for  $CT_n$  which describes the energy of  $CT_n$ , and  $\hat{H}_{ET} = \hat{H}_{LE,CT} + \hat{H}_{CT,GS}$ .  $\Delta\hat{V}_{LE_n}^{b_{LE_n}} = \hat{V}_{LE_n} - \hat{V}_0$  describes how the potential energy surface of the ground state is perturbed by the electronic excitation  $LE_n$ , and similarly  $\Delta\hat{V}_{CT_n}^{b_{CT_n}} + \sum_m \Delta\hat{V}_{CT_n}^{b_{LE_m}} = \hat{V}_{CT_n} - \hat{V}_0$  describes how the ground state potential is shifted in the charge transfer state  $CT_n$ . The potential energy shift for the CT states are divided into a sum of terms which are correlated with the  $LE_m$  energy shifts,  $\Delta\hat{V}_{CT_n}^{b_{LE_m}}$ , corresponding to reorganization of the intramolecular modes on each chromophore, and the remaining uncorrelated component  $\Delta\hat{V}_{CT_n}^{b_{CT_n}}$ . The reference ground state potentials for the  $b_{LE}$  and  $b_{CT}$  degrees of freedom are given by  $\hat{H}_{GS}^{b_{LE}}$  and  $\hat{H}_{GS}^{b_{CT}}$  respectively.

## B. The LE state potential energy surfaces

We can often assume that the LE state energy shift operators  $\Delta\hat{V}_{LE_n}^{b_{LE_n}}$  have Gaussian statistics in the ground state reference ensemble, meaning third-order cumulants and higher vanish. Further we assume correlation functions of  $\Delta\hat{V}_{LE_n}^{b_{LE_n}}$  can be decomposed into a sum of contributions as follows<sup>12,14</sup>

$$\left\langle \Delta\hat{V}_{LE_n}^{b_{LE_n}}(t) \Delta\hat{V}_{LE_m}^{b_{LE_m}}(0) \right\rangle_{b_{LE}} = \delta_{n,m} \sum_{r=1}^{N_{b,n}} C_{n,r}(t) \quad (13)$$

where  $\langle \dots \rangle_{b_{LE}} = \text{Tr}_{b_{LE}}[\dots e^{-\beta\hat{H}_{GS}^{b_{LE}}}] / \text{Tr}_{b_{LE}}[e^{-\beta\hat{H}_{GS}^{b_{LE}}}]$ , and  $\Delta\hat{V}_{LE_n}^{b_{LE_n}}(t) = e^{i\hat{H}_{GS}^{b_{LE}}t/\hbar} \Delta\hat{V}_{LE_n}^{b_{LE_n}} e^{-i\hat{H}_{GS}^{b_{LE}}t/\hbar}$ . Provided  $C_{n,r}(t)$  is a smooth function it can be written in terms of a spectral density  $\mathcal{J}_{n,r}(\omega)$  as

$$C_{n,r}^{b_{LE}}(t) = \frac{\hbar}{\pi} \int_0^\infty d\omega \mathcal{J}_{n,r}(\omega) \left[ \coth\left(\frac{\beta\hbar\omega}{2}\right) \cos(\omega t) - i \sin(\omega t) \right]. \quad (14)$$

With these assumptions,  $\hat{H}_{GS}^{b_{LE}}$  can be written as a sum of independent harmonic bath Hamiltonians, and that the LE state energy shift terms  $\Delta\hat{V}_{LE_n}^{b_{LE_n}}$  are linear in the bath mode displacements.<sup>13</sup> These assumptions are widely used in describing exciton dynamics, and largely hold due to the relatively weak coupling between the LE states and the environment, meaning shifts in the potential energy surfaces can be

well approximated as simple shifts in a harmonic potential.<sup>1,12</sup> Overall this means we can write the b<sub>LE</sub> Hamiltonians as<sup>12</sup>

$$\hat{H}_{\text{GS}}^{\text{bLE}} = \sum_{n=1}^{N_{\text{LE}}} \sum_{r=1}^{N_{\text{b},n}} \sum_{\alpha=1}^{N_{n,r}} \left( \frac{\hat{p}_{nr\alpha}^2}{2m_{nr\alpha}} + \frac{1}{2} m_{nr\alpha} \omega_{nr\alpha}^2 \hat{q}_{nr\alpha}^2 \right) \quad (15)$$

$$\Delta \hat{V}_{\text{LE}_n}^{\text{bLE}_n} = \sum_{r=1}^{N_{\text{b},n}} \hat{B}_{n,r} = \sum_{r=1}^{N_{\text{b},n}} \sum_{\alpha=1}^{N_{n,r}} c_{nr\alpha} \hat{q}_{nr\alpha} \quad (16)$$

where the bath mode frequencies  $\omega_{nr\alpha}$  and coupling coefficients  $c_{nr\alpha}$  of the mode displacement operators  $\hat{q}_{nr\alpha}$  appear in the bath coupling operators  $\hat{B}_{nr\alpha}$ . We can evaluate the spectral density

$$\mathcal{J}_{n,r}(\omega) = \frac{\pi}{2} \sum_{\alpha=1}^{N_{n,r}} \frac{c_{nr\alpha}^2}{m_{nr\alpha} \omega_{nr\alpha}} \delta(\omega - \omega_{nr\alpha}) \quad (17)$$

in terms of these microscopic parameters in the Hamiltonian.

### C. The hierarchical equations of motion

The hierarchical equations of motion provide a method for simulating the dynamics of a system linearly coupled to a harmonic bath. It was developed for Hamiltonians like those that we are interested in that can be decomposed as<sup>13</sup>

$$\hat{H} = \hat{H}_s + \sum_{j=1}^{N_b} (\hat{H}_{b,j} + \hat{V}_j \hat{B}_j). \quad (18)$$

where  $\hat{H}_s$  is the sub-system Hamiltonian,  $\hat{V}_j$  are system operators,  $\hat{H}_{b,j}$  is the Hamiltonian of harmonic bath  $j$ . The bath displacement operators,  $\hat{B}_j$ , are defined as,  $\hat{H}_{b,j} = \sum_{\alpha=1}^{N_j} \hat{p}_{j\alpha}^2 / 2m_{j\alpha} + m_{j\alpha} \omega_{j\alpha}^2 \hat{q}_{j\alpha}^2 / 2$  and  $\hat{B}_j = \sum_{\alpha=1}^{N_j} c_{j,\alpha} \hat{q}_{j,\alpha}$  as analogous to Eqs. (15) and (16) where the index  $n, r$  is replaced with a single index  $j$ . Assuming the bath displacement operator correlation functions can be decomposed as

$$C_j(t) = \sum_{k=1}^{\infty} a_{jk} e^{-\nu_{jk} t} \quad (19)$$

and using the Gaussian property of the harmonic baths, we can obtain the system reduced density operator  $\hat{\rho}(t) = \text{Tr}_b[\hat{\rho}_{\text{tot}}(t)]$ , from a hierarchy of auxiliary density operators (ADOs)  $\hat{\rho}_{\mathbf{n}}(t)$  which obey the following equation of motion,<sup>11,13,68</sup>

$$\begin{aligned} \frac{d}{dt} \hat{\rho}_{\mathbf{n}}(t) = & -\frac{i}{\hbar} [\hat{H}_s, \hat{\rho}_{\mathbf{n}}(t)] - \sum_{j,k} n_{jk} \nu_{jk} \hat{\rho}_{\mathbf{n}}(t) + \Xi_{\mathbf{n}} \hat{\rho}_{\mathbf{n}}(t) \\ & - \frac{i}{\hbar} \sum_{j,k} \sqrt{(n_{jk} + 1)} |a_{jk}| [\hat{V}_j, \hat{\rho}_{\mathbf{n}_{jk}^+}] \\ & - \frac{i}{\hbar} \sum_{j,k} \sqrt{\frac{n_{jk}}{|a_{jk}|}} (a_{jk} \hat{V}_j \hat{\rho}_{\mathbf{n}_{jk}^-} - a_{jk}^* \hat{\rho}_{\mathbf{n}_{jk}^-} \hat{V}_j). \end{aligned} \quad (20)$$

where  $\mathbf{n} = (n_{1,0}, n_{1,1}, \dots, n_{j,k}, \dots)$  is a multi-index that specifies the excitation level of mode  $k$  for each bath  $j$  for a given

hierarchy element,  $\mathbf{n}_{jk}^{\pm} = (n_{1,0}, n_{1,1}, \dots, n_{j,k} \pm 1, \dots)$ , and  $\Xi_{\mathbf{n}}$  is a system superoperator that accounts for finite truncation of the hierarchy. The sub-system reduced density operator can be obtained as the zeroth element of this hierarchy  $\hat{\rho}(t) = \hat{\rho}_{\mathbf{0}}(t)$ .

We can write down the truncated hierarchy as

$$|\rho(t)\rangle\rangle = \sum_{\mathbf{n}} |\rho_{\mathbf{n}}(t)\rangle\rangle \otimes |\mathbf{n}\rangle\rangle \quad (21)$$

where  $|\mathbf{n}\rangle\rangle$  is a basis vector corresponding to auxiliary density operator  $\mathbf{n}$ , and  $|\rho_{\mathbf{n}}(t)\rangle\rangle$  is the Liouville space vector of this ADO. With this notation we can write down the equation of motion more compactly as<sup>29,33,69</sup>

$$\frac{d}{dt} |\rho(t)\rangle\rangle = \mathcal{L} |\rho(t)\rangle\rangle \quad (22)$$

$$= (\mathcal{L}_s \otimes \mathcal{I}_{\text{ado}} - \mathcal{I}_s \otimes \Gamma + \Xi + \mathcal{V}) |\rho(t)\rangle\rangle \quad (23)$$

where  $\mathcal{L}_s = -(i/\hbar)[\hat{H}_s, \cdot]$  is the system Liouvillian,  $\mathcal{I}_s$  and  $\mathcal{I}_{\text{ado}}$  are identity operators on the system Liouville space and the set of ADOs respectively,  $\Gamma = \sum_{\mathbf{n}} \gamma_{\mathbf{n}} |\mathbf{n}\rangle\rangle \langle\langle \mathbf{n}|$  is a matrix of ADO decay rates,  $\Xi = \sum_{\mathbf{n} \in \mathcal{N}} \Xi_{\mathbf{n}} \otimes |\mathbf{n}\rangle\rangle \langle\langle \mathbf{n}|$  is superoperator that accounts for finite truncation of the hierarchy<sup>68</sup>, and  $\mathcal{V}$  is the term that couples different ADOs within the hierarchy. Henceforth we will swap between Liouville vector notation  $|\rho\rangle\rangle$  and standard operator notation  $\hat{\rho}$ , as is most appropriate.

### III. THE HYBRID HEOM/QME METHOD

Using HEOM to study CT in these systems can be difficult due to the large reorganization energies, which give rise to large values of  $a_{jk}$  for baths associated with CT processes. The large coupling coefficients for certain modes means many ADOs are needed to converge the HEOM dynamics. This can make HEOM calculations involving CT states intractable when there are large numbers of system states and baths. A simplification results as the reorganization energy of charge transfer processes is typically much larger than the electronic coupling between CT states and LE states, the use of perturbation theory, where the coupling to the CT states is treated as a small parameter, can be expected to give an accurate description of the coupled dynamics of the LE and CT states.<sup>27,51,52</sup> In this section, we describe how Zwanzig projection can be used to construct a hybrid HEOM/QME method in which radiative and electron transfer processes are treated with perturbation theory while preserving the high accuracy of the EET dynamics afforded by HEOM. Similar approaches have been used to derive hybrid HEOM methods to describe radiative processes in EET in protein-pigment complexes,<sup>19,23,70</sup> but these have not included charge transfer processes. The approach taken here combines some of the ideas for describing radiative processes in Ref. 19 with Nakajima-Zwanzig theory based approaches that have been used to derive quantum master equations for spin density operators of different charge transfer states in photo-excited molecules.<sup>51-53</sup>

### A. Zwanzig projection

Here we use the Zwanzig projection operator approach to construct a hybrid HEOM/QME method. We set up the problem by formally including the  $b_{CT}$  and EM field degrees of freedom, as well as the full set of electronic states, in the system Hamiltonian  $\hat{H}_s$  in the hierarchical equations of motion. This means the “system” Hamiltonian is taken to be

$$\hat{H}_s = \hat{H}_{LE,s} + \sum_{n=1}^{N_{CT}} \Pi_{CT_n} \left( \hat{H}_{CT_n,s} + \Delta \hat{V}_{CT_n}^{b_{CT}} \right) + \hat{H}_{GS}^{b_{CT}} + \hat{H}_{LE,CT} + \hat{H}_{CT,GS} + \hat{H}_{EM} + \hat{H}_D. \quad (24)$$

The response of the system to the  $b_{LE}$  couplings is treated with the HEOM, with the set of  $N_{b_{LE}} = \sum_n N_{b,n}$  baths indexed by  $j = n, r$ , and

$$\hat{V}_{n,r} = |\text{LE}_n\rangle\langle\text{LE}_n| + \sum_{m=1}^{N_{CT}} \kappa_{n,r}^{CT_m} \hat{\Pi}_{CT_m}, \quad (25)$$

are the set of system-bath coupling operators. The coefficients  $\kappa_{n,r}^{CT_m}$  here describe how the  $b_{LE}$  degrees of freedom are coupled to the CT states.

The main variables of interest for this system are the reduced density operator for the LE states, and the CT and GS state populations. These populations are given by

$$\hat{\sigma}_{A,s}(t) = \hat{\Pi}_A \text{Tr}_b[\hat{\rho}_0(t)] \hat{\Pi}_A \quad (26)$$

where  $\hat{\Pi}_A$  is a projection operator onto the manifold of electronic states with  $A = \text{LE}, \text{CT}_n$  or  $\text{GS}$ , and  $\text{Tr}_b$  denotes a trace over all  $b_{CT}$  and  $b_{EM}$  field degrees of freedom. Since we aim to treat the exciton dynamics with the HEOM, we construct the projection operator for the HEOM ADOs as

$$\mathcal{P} = \sum_A \mathcal{P}_A \otimes \mathcal{I}_{\text{ado}} \quad (27)$$

$$\mathcal{P}_A = \hat{\rho}_A^{b_{CT}} \hat{\rho}^{b_{EM}} \hat{\Pi}_A \text{Tr}_b[\cdot] \hat{\Pi}_A \quad (28)$$

where local equilibrium density operator for the  $b_{CT}$  degrees of freedom in state  $A$  is  $\hat{\rho}_A^{b_{CT}} = e^{-\beta \hat{H}_A^{b_{CT}}} / \text{Tr}_{b_{CT}}[e^{-\beta \hat{H}_A^{b_{CT}}}]$ , and  $\hat{H}_A^{b_{CT}} = \hat{H}_{GS}^{b_{CT}}$  for  $A = \text{GS}$  or  $\text{LE}$ , and  $\hat{H}_{CT_n}^{b_{CT}} = \hat{H}_{GS}^{b_{CT}} + \Delta \hat{V}_{CT_n}^{b_{CT}}$ . The EM field density operator is approximated as the zero temperature equilibrium density operator of the bare EM field, where all field modes are in their ground-state,  $\hat{\rho}^{b_{EM}} = \bigotimes_{k,p} |0_{k,p}\rangle\langle 0_{k,p}|$ . This approximation is justified by the fact that we are only interested in spontaneous emission processes, since field modes at the LE state energies are not thermally excited at ambient temperatures, therefore  $\beta \hbar \omega_{k,p} \approx 0$  for field modes resonant with the LE-GS energy gaps. This type of projection operator is analogous to that used in Refs. 51 and 52 for electronic state spin density operators. This projected density operator contains the reduced density operator hierarchy,

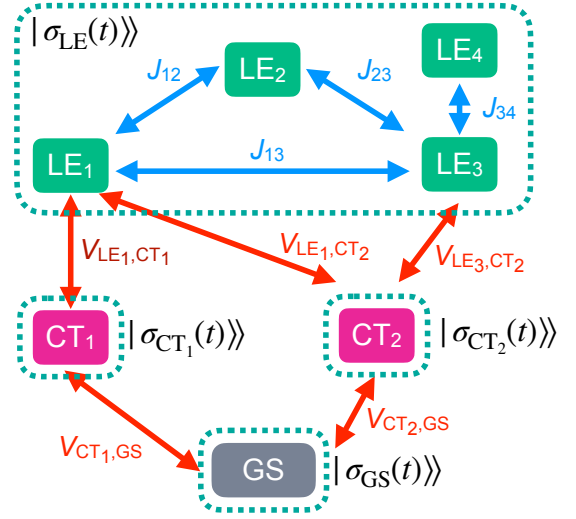


FIG. 2. An schematic of the states, interstate coupling, and partitioning into reduced hierarchies  $|\sigma_A(t)\rangle\rangle$  for an example system with four LE states, two CT states and the GS.

$|\sigma_A(t)\rangle\rangle$ , for each electronic state  $A$ ,

$$\mathcal{P}|\rho(t)\rangle\rangle = \sum_A |\rho_A^{b_{CT}}\rangle\rangle \otimes |\rho^{b_{EM}}\rangle\rangle \otimes |\sigma_A(t)\rangle\rangle \quad (29)$$

$$|\sigma_A(t)\rangle\rangle = \sum_{\mathbf{n}} |\sigma_{A,\mathbf{n}}(t)\rangle\rangle \otimes |\mathbf{n}\rangle\rangle \quad (30)$$

$$\hat{\sigma}_{A,\mathbf{n}}(t) = \hat{\Pi}_A \text{Tr}_b[\hat{\rho}_{\mathbf{n}}(t)] \hat{\Pi}_A. \quad (31)$$

An example of the partitioning into separate hierarchies for different state manifolds,  $|\sigma_A(t)\rangle\rangle$ , is illustrated in Fig. 2 for system with four LE states, two CT states and the ground state.

Using this projection operator  $\mathcal{P}$  we can obtain a quantum master equation for the projected hierarchy of ADOs  $\mathcal{P}|\rho(t)\rangle\rangle$  using the Nakajima-Zwanzig equation<sup>58–60</sup>

$$\frac{d}{dt} \mathcal{P}|\rho(t)\rangle\rangle = \mathcal{P} \mathcal{L} \mathcal{P} |\rho(t)\rangle\rangle + \int_0^t \mathcal{K}(t-\tau) \mathcal{P} |\rho(\tau)\rangle\rangle d\tau, \quad (32)$$

where the memory kernel  $\mathcal{K}(t)$  is given by

$$\mathcal{K}(t) = \mathcal{P} \mathcal{L} e^{(1-\mathcal{P})\mathcal{L}t} (1-\mathcal{P}) \mathcal{L} \mathcal{P}. \quad (33)$$

The generalized master equations for  $|\sigma_A(t)\rangle\rangle$  can be straightforwardly obtained from this by tracing out the  $b_{CT}$  and  $b_{EM}$  degrees of freedom. This gives the following general hybrid HEOM/QME for  $|\sigma_A(t)\rangle\rangle$ ,

$$\frac{d}{dt} |\sigma_A(t)\rangle\rangle = \mathcal{L}_A |\sigma_A(t)\rangle\rangle + \sum_B \int_0^t \mathcal{K}_{AB}(t-\tau) |\sigma_B(\tau)\rangle\rangle d\tau. \quad (34)$$

where  $\mathcal{L}_A = \langle\langle 1_b | \mathcal{P}_A \mathcal{L} \mathcal{P}_A | \rho_A^b \rangle\rangle$  is the component of  $\mathcal{P} \mathcal{L} \mathcal{P}$  that acts on  $|\sigma_A(t)\rangle\rangle$  and similarly  $\mathcal{K}_{AB}(t)$  is the component of  $\mathcal{K}_{AB}(t) = \langle\langle 1_b | \mathcal{P}_A \mathcal{K}(t) \mathcal{P}_B | \rho_B^b \rangle\rangle$  that couples  $|\sigma_B(t)\rangle\rangle$  to  $|\sigma_A(t)\rangle\rangle$ . Here  $|1_b\rangle\rangle$  is the identity operator on the  $b_{CT}$  and  $b_{EM}$  degrees of freedom and  $|\rho_A^b\rangle\rangle = |\rho_A^{b_{CT}}\rangle\rangle \otimes |\rho^{b_{EM}}\rangle\rangle$ , and the Liouville space inner product is  $\langle\langle A | B \rangle\rangle = \text{Tr}[\hat{A}^\dagger \hat{B}]$ .

## B. Approximating the exact master equation

While Eq. (34) is formally exact, evaluating the kernel requires evaluation of the exact dynamics generated by  $\mathcal{L}$ , which due to the large Hilbert space associated with  $\mathbf{b}_{\text{CT}}$  and  $\mathbf{b}_{\text{EM}}$  is difficult. However, in the absence of the excitonic dynamics, each would be able to be treated accurately with simplifying approximations. Firstly, we make the Markovian approximation, in which we assume the decay time-scale of  $\mathcal{K}_{AB}(t)$  is much faster than the dynamics of  $|\sigma_A(t)\rangle\rangle$ , and therefore we approximate the time-convolution terms as<sup>50,51</sup>

$$\int_0^t \mathcal{K}_{AB}(t-\tau) |\sigma_B(\tau)\rangle\rangle d\tau \approx \int_0^\infty \mathcal{K}_{AB}(\tau) d\tau |\sigma_B(t)\rangle\rangle. \quad (35)$$

Secondly, we approximate the full kernel in Eq. (33) with its second order approximation in perturbation theory.<sup>50,51</sup> Here the perturbation Liouvillian  $\mathcal{L}_V$  is taken to be

$$\mathcal{L}_V = \mathcal{L}_{\text{ET}} + \mathcal{L}_R \quad (36)$$

$$\mathcal{L}_{\text{ET}} = -\frac{i}{\hbar} [\hat{H}_{\text{ET}}, \cdot] \otimes \mathcal{I}_{\text{ado}} \quad (37)$$

$$\mathcal{L}_R = -\frac{i}{\hbar} [\hat{H}_D, \cdot] \otimes \mathcal{I}_{\text{ado}}, \quad (38)$$

and with this the kernel  $\mathcal{K}(t)$  can be approximated as

$$\mathcal{K}(t) \approx \mathcal{K}^{(2)}(t) = \mathcal{P} \mathcal{L}_V e^{(\mathcal{L}_0 + \mathcal{V})t} \mathcal{L}_V \mathcal{P}, \quad (39)$$

where we have defined  $\mathcal{L}_0 = \mathcal{L} - \mathcal{L}_V - \mathcal{V}$ . Because the baths are uncorrelated, the second order kernel can be split into

$$\begin{aligned} \mathcal{K}^{(2)}(t) &= \mathcal{K}_{\text{ET}}^{(2)}(t) + \mathcal{K}_R^{(2)}(t) \\ &= \mathcal{P} \mathcal{L}_{\text{ET}} e^{(\mathcal{L}_0 + \mathcal{V})t} \mathcal{L}_{\text{ET}} \mathcal{P} + \mathcal{P} \mathcal{L}_R e^{(\mathcal{L}_0 + \mathcal{V})t} \mathcal{L}_R \mathcal{P} \end{aligned} \quad (41)$$

an electron transfer term,  $\mathcal{K}_{\text{ET}}^{(2)}(t)$  and a radiative decay term,  $\mathcal{K}_R^{(2)}(t)$ .

The final simplification we make is to approximate the reference propagator  $e^{(\mathcal{L}_0 + \mathcal{V})t}$  appearing in the ET kernel as

$$e^{(\mathcal{L}_0 + \mathcal{V})t} \approx e^{(\mathcal{L}_0 + \tilde{\mathcal{V}})t} \quad (42)$$

where  $\tilde{\mathcal{V}} = \sum_{\mathbf{n}, \mathbf{n}' \in \mathcal{N}_K} |\mathbf{n}\rangle\rangle\langle\langle \mathbf{n}'| \mathcal{V} |\mathbf{n}'\rangle\rangle\langle\langle \mathbf{n}|$  is  $\mathcal{V}$  projected onto a subset of the ADOs. We make this approximation to reduce the density of the coupling between elements of  $|\sigma_A(t)\rangle\rangle$  in the equations of motion, and increase the computational efficiency of the method. For the radiative decay term we simply approximate  $e^{(\mathcal{L}_0 + \mathcal{V})t} \approx e^{\mathcal{L}_0 t}$ , where  $\mathcal{L}_0$  is just the coherent system dynamics term appearing in  $\mathcal{L}_0$ . In deriving explicit expressions for terms appearing in the hybrid HEOM/QME, it is important to note that  $\mathcal{L}_0$  and  $\mathcal{V}$  can be decomposed as  $\mathcal{L}_0 = \bigoplus_{A,B} \mathcal{L}_0^{AB}$  and  $\mathcal{V} = \bigoplus_{A,B} \mathcal{V}^{AB}$ , where each term only acts on coherences  $|A\rangle\langle B|$  between electronic states in manifolds  $A$  and  $B$ .

Applying the above set of approximations to Eq. (34), allows us to write the hybrid HEOM/QME as

$$\frac{d}{dt} |\sigma_A(t)\rangle\rangle = \mathcal{L}_A |\sigma_A(t)\rangle\rangle + \sum_B \mathcal{R}_{AB} |\sigma_B(t)\rangle\rangle, \quad (43)$$

where  $\mathcal{R}_{AB}$  can be written as a sum of electron transfer and radiative decay terms,  $\mathcal{R}_{AB} = \mathcal{R}_{AB}^{\text{ET}} + \mathcal{R}_{AB}^{\text{R}}$ . We can write this system of equations more explicitly as

$$\begin{aligned} \frac{d}{dt} \hat{\sigma}_{A,\mathbf{n}}(t) &= -\frac{i}{\hbar} [\hat{H}_{A,s}, \hat{\sigma}_{A,\mathbf{n}}(t)] - \gamma_{\mathbf{n}} \hat{\sigma}_{A,\mathbf{n}}(t) \\ &+ \Xi_{A,\mathbf{n}} \hat{\sigma}_{A,\mathbf{n}}(t) - \frac{i}{\hbar} \sum_{j,k} \sqrt{(n_{jk} + 1) |a_{jk}|} [\hat{V}_{A,j}, \hat{\sigma}_{A,\mathbf{n}_{jk}^+}(t)] \\ &- \frac{i}{\hbar} \sum_{j,k} \sqrt{\frac{n_{jk}}{|a_{jk}|}} \left( a_{jk} \hat{V}_{A,j} \hat{\sigma}_{A,\mathbf{n}_{jk}^-}(t) - a_{jk}^* \hat{\sigma}_{A,\mathbf{n}_{jk}^-}(t) \hat{V}_{A,j} \right) \\ &+ \sum_B \sum_{\mathbf{n}'} \mathcal{R}_{AB,\mathbf{nn}'} \hat{\sigma}_{B,\mathbf{n}'}(t), \end{aligned} \quad (44)$$

where  $\hat{H}_{A,s}$  and  $\hat{V}_A$  are the components of the electronic state terms in  $\hat{H}_s$  and  $\hat{V}$  projected onto the manifold of electronic states  $A$ ,  $\Xi_{A,\mathbf{n}}$  is superoperator that accounts for finite truncation, projected on  $A$ , and  $\mathcal{R}_{AB,\mathbf{nn}'}$  is the component of  $\mathcal{R}_{AB}$  that couples state  $\hat{\sigma}_{A,\mathbf{n}}(t)$  to  $\hat{\sigma}_{B,\mathbf{n}'}(t)$ . Now that we have the general form of the Markovian hybrid HEOM/QME, we just need to evaluate the transfer operators  $\mathcal{R}_{AB}^{\text{ET}}$  and  $\mathcal{R}_{AB}^{\text{R}}$ . This is detailed in the following sections.

## C. The electron transfer term

We start by considering the electron transfer term,  $\mathcal{R}_{AB}^{\text{ET}}$ . By noting that  $\mathcal{L}_0 + \tilde{\mathcal{V}}$  does not mix populations and coherences between the LE, CT and GS manifolds, the elements of  $\mathcal{R}_{AB}^{\text{ET}}$  where  $A \neq B$  can be evaluated straightforwardly as

$$\mathcal{R}_{AB}^{\text{ET}} = \mathcal{L}_{\text{HET}}^{\text{L},AB} \mathcal{G}_{AB}^B \mathcal{L}_{\text{HET}}^{\text{R},BA} + \mathcal{L}_{\text{HET}}^{\text{R},BA} \mathcal{G}_{BA}^B \mathcal{L}_{\text{HET}}^{\text{L},AB}. \quad (45)$$

where the  $\mathcal{L}_{\text{HET}}^{\text{L,R},AB}$  terms are given by

$$\mathcal{L}_{\text{HET}}^{\text{L},AB} \hat{\sigma} = \frac{1}{\hbar} \hat{\Pi}_A \hat{H}_{\text{ET}} \hat{\Pi}_B \hat{\sigma} \quad (46)$$

$$\mathcal{L}_{\text{HET}}^{\text{R},BA} \hat{\sigma} = \frac{1}{\hbar} \hat{\sigma} \hat{\Pi}_B \hat{H}_{\text{ET}} \hat{\Pi}_A \quad (47)$$

and the  $\mathcal{G}_{AB}^C$  terms are given by

$$\mathcal{G}_{AB}^B = \int_0^\infty dt G_{AB}^B(t) \mathcal{S}_{AB}^{\text{ET}} e^{\Lambda_{AB}^{\text{ET}} t} \mathcal{S}_{AB}^{\text{ET}-1} \quad (48)$$

where we have used the spectral decomposition of the projected reference Liouvillian

$$(\mathcal{L}_0^{AB} + \tilde{\mathcal{V}}_{\text{ET}}^{AB}) \mathcal{S}_{AB}^{\text{ET}} = \Lambda_{AB}^{\text{ET}} \mathcal{S}_{AB}^{\text{ET}} \quad (49)$$

where  $\mathcal{L}_0^{AB}$  is defined as the block of  $\mathcal{L}_0$  that just acts on  $AB$  coherences, and likewise for  $\tilde{\mathcal{V}}_{\text{ET}}^{AB}$ , and  $\mathcal{S}_{AB}^{\text{ET}}$  is the matrix of eigenvectors and  $\Lambda_{AB}^{\text{ET}}$  is the diagonal matrix of eigenvalues. Due to the block diagonal structure of  $\mathcal{L}_0^{AB} + \tilde{\mathcal{V}}_{\text{ET}}^{AB}$  this can be straightforwardly evaluated. The correlation function  $G_{AB}^C(t)$  is given by

$$G_{AB}^C(t) = \text{Tr}_{\mathbf{b}_{\text{CT}}} [e^{-i\hat{H}_A^{\text{bCT}} t/\hbar} e^{+i\hat{H}_B^{\text{bCT}} t/\hbar} \hat{\rho}_C^{\text{bCT}}]. \quad (50)$$

which is the moment generating function for the energy gap between subsystems  $A$  and  $B$ . The remaining diagonal  $\mathcal{R}_{AA}^{\text{ET}}$  terms are given by

$$\mathcal{R}_{AA}^{\text{ET}} = - \sum_{B \neq A} \left( \mathcal{L}_{\text{HET}}^{\text{L},BA} \mathcal{G}_{BA}^A \mathcal{L}_{\text{HET}}^{\text{L},BA} + \mathcal{L}_{\text{HET}}^{\text{R},AB} \mathcal{G}_{AB}^A \mathcal{L}_{\text{HET}}^{\text{R},AB} \right) \quad (51)$$

as required to conserve population.

For practical calculations we use the full version of these expressions, but insight into the effect of ET on the exciton dynamics can be gained by making some additional approximations. First we consider the limit where the system and LE bath time-scales are long compared to the decay time of  $G_{\text{CT,LE}}^{\text{LE}}(t)$ . In this limit the  $\mathcal{R}_{\text{LE,LE}}^{\text{ET}}$  term becomes

$$\mathcal{R}_{\text{LE,LE}}^{\text{ET}} = - \sum_{n=1}^{N_{\text{CT}}} \frac{k_{\text{CT}_n \leftarrow \text{LE}}}{2} \{ \hat{P}_n, \cdot \} - \frac{i}{\hbar} \sum_{n=1}^{N_{\text{CT}}} \Delta_n [ \hat{P}_n, \cdot ] . \quad (52)$$

a sum of dissipative and conservative terms. Here,  $k_{\text{CT}_n \leftarrow \text{LE}}$  is the Fermi's Golden Rule rate constant for ET from the LE manifold to the  $\text{CT}_n$  state,<sup>50</sup>

$$k_{\text{CT}_n \leftarrow \text{LE}} = \frac{|V_{\text{CT}_n \leftarrow \text{LE}}|^2}{\hbar^2} \int_{-\infty}^{\infty} G_{\text{CT,LE}}^{\text{LE}}(t) e^{-i(E_{\text{CT}_n} - \bar{E}_{\text{LE}})t/\hbar} dt \quad (53)$$

and  $\bar{E}_{\text{LE}}$  is an effective energy scale of the LE states such that  $\hat{H}_{\text{LE},s} \approx \bar{E}_{\text{LE}} \hat{\Pi}_{\text{LE}}$ ,  $\hat{H}_{\text{CT}_n,s} = E_{\text{CT}_n} \hat{\Pi}_{\text{CT}_n}$ , with the effective coupling constant

$$|V_{\text{CT}_n \leftarrow \text{LE}}|^2 = \sum_{m=1}^{N_{\text{LE}}} |V_{\text{LE}_m, \text{CT}_n}|^2 \quad (54)$$

is given by a sum over all of the LE states. Finally,  $\hat{P}_n = |\psi_n\rangle\langle\psi_n|$  is a projection operator onto the reactive state in the LE manifold which is given by

$$|\psi_n\rangle = \frac{1}{|V_{\text{CT}_n \leftarrow \text{LE}}|} \sum_{m=1}^{N_{\text{LE}}} |LE_m\rangle V_{\text{LE}_m, \text{CT}_n}, \quad (55)$$

and  $\Delta_n$  is an energy shift term,

$$\Delta_n = \frac{|V_{\text{CT}_n \leftarrow \text{LE}}|^2}{\hbar} \text{Im} \int_0^{\infty} G_{\text{CT,LE}}^{\text{LE}}(t) e^{-i(E_{\text{CT}_n} - \bar{E}_{\text{LE}})t/\hbar} dt \quad (56)$$

which in the limit of a highly activated reaction is given by

$$\Delta_n \approx \frac{|V_{\text{CT}_n \leftarrow \text{LE}}|^2}{\Delta E_{\text{CT}_n \leftarrow \text{LE}}} \quad (57)$$

where  $\Delta E_{\text{CT}_n \leftarrow \text{LE}}$  is the vertical energy gap from the LE state to the  $\text{CT}_n$  state.<sup>51,53</sup>

From this we deduce that electron transfer has three main effects on the exciton dynamics. Firstly the ET causes population loss from the LE manifold from the reactive state  $|\psi_n\rangle$ . Secondly it causes decoherence between the states  $|\psi_n\rangle$  state and the rest of the manifold of LE states. Thirdly, the energy

shift terms perturb the exciton dynamics, modifying the energy gaps and couplings between LE states. If the reactive state is just a specific localized LE state, i.e.  $|\psi_n\rangle = |LE_{r_n}\rangle$ , then the energy shift term just alters the energy of this LE state, which in the excitonic basis introduces coupling between delocalized excitonic states, as well as shifting exciton state energies. In the limit of Gaussian statistics for the bath and high temperature, this reduces to Marcus theory.<sup>50,71,72</sup> Eq. (53) ignores the effect of exciton formation, which shifts the free energy of states in the LE manifold, thereby changing the rate constants for electron transfer. The full hybrid HEOM/QME theory that we use in simulations however includes this important effect.

#### D. The radiative decay term

The radiative coupling terms can be derived in a similar manner to the ET term, details of which are given in the appendix. Here we simply state the final expressions for the two non-zero radiative transfer terms  $\mathcal{R}_{\text{GS,LE}}^{\text{R}}$  and  $\mathcal{R}_{\text{LE,LE}}^{\text{R}}$ . The  $\text{GS} \leftarrow \text{LE}$  transfer term is given by

$$\mathcal{R}_{\text{GS,LE}}^{\text{R}} = \frac{1}{6\hbar\epsilon_0 c_0^3 \pi} \sum_{\alpha=x,y,z} \left( \mathcal{L}_{\alpha}^{\text{L}} \mathcal{S}_{\text{LE,GS}}^{0,s} \Omega_{\text{LE,GS}}^3 (\mathcal{S}_{\text{LE,GS}}^{0,s})^{-1} \mathcal{L}_{\alpha}^{\text{R}} + \mathcal{L}_{\alpha}^{\text{R}} \mathcal{S}_{\text{GS,LE}}^{0,s} \Omega_{\text{GS,LE}}^3 (\mathcal{S}_{\text{GS,LE}}^{0,s})^{-1} \mathcal{L}_{\alpha}^{\text{L}} \right). \quad (58)$$

and similarly the  $\mathcal{R}_{\text{LE,LE}}^{\text{R}}$  term can be evaluated as

$$\mathcal{R}_{\text{LE,LE}}^{\text{R}} = - \frac{1}{6\hbar\epsilon_0 c_0^3 \pi} \sum_{\alpha=x,y,z} \left( \mathcal{L}_{\alpha}^{\text{R}} \mathcal{S}_{\text{LE,GS}}^{0,s} \Omega_{\text{LE,GS}}^3 (\mathcal{S}_{\text{LE,GS}}^{0,s})^{-1} \mathcal{L}_{\alpha}^{\text{R}} + \mathcal{L}_{\alpha}^{\text{L}} \mathcal{S}_{\text{GS,LE}}^{0,s} \Omega_{\text{GS,LE}}^3 (\mathcal{S}_{\text{GS,LE}}^{0,s})^{-1} \mathcal{L}_{\alpha}^{\text{L}} \right). \quad (59)$$

where  $\mathcal{L}_{\alpha}^{\text{L}} \hat{\sigma} = \hat{\Pi}_{\text{GS}} \hat{\mu}_{\alpha} \hat{\Pi}_{\text{LE}} \hat{\sigma}$  and  $\mathcal{L}_{\alpha}^{\text{R}} \hat{\sigma} = \hat{\sigma} \hat{\Pi}_{\text{LE}} \hat{\mu}_{\alpha} \hat{\Pi}_{\text{GS}}$ . These expressions use the eigenvalue decompositions of the blocks of  $\mathcal{L}_{0,s}$ ,  $\mathcal{L}_{0,s}^{\text{GS,LE}} = \mathcal{S}_{\text{GS,LE}}^{0,s} (i\Omega_{\text{GS,LE}}) (\mathcal{S}_{\text{GS,LE}}^{0,s})^{-1}$  and  $\mathcal{L}_{0,s}^{\text{LE,GS}} = \mathcal{S}_{\text{LE,GS}}^{0,s} (-i\Omega_{\text{LE,GS}}) (\mathcal{S}_{\text{LE,GS}}^{0,s})^{-1}$ , where  $\Omega_{\text{GS,LE}}$  and  $\Omega_{\text{LE,GS}}$  are diagonal matrices with real positive-valued entries. It should be noted that the decay rates for the excitonic states  $|\epsilon_n\rangle$  appearing in these expressions exactly correspond to the standard Wigner-Weisskopf decay rates.<sup>23</sup>

#### IV. EXCITON DIMER MODEL

As a test for the approximations that go into the hybrid HEOM/QME method, we have performed simulations on a model exciton dimer, consisting of two LE states, coupled to a single CT state. The  $\text{b}_{\text{CT}}$  bath is taken to be harmonic in this example, allowing us to obtain exact dynamics directly with the HEOM method. The LE system Hamiltonian for this

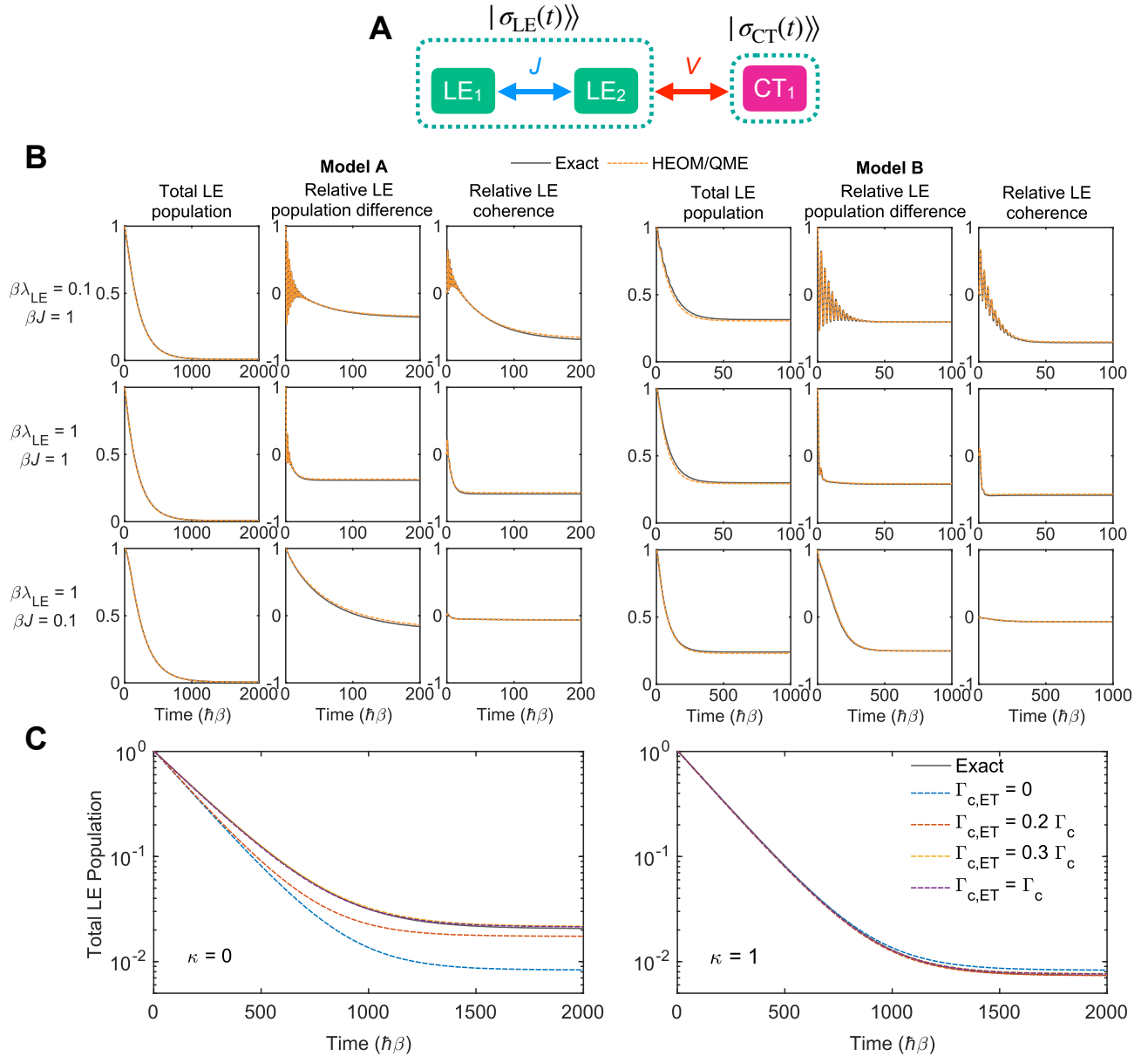


FIG. 3. A: Schematic diagram showing the LE states and CT state in the dimer model, and the non-zero interstate couplings, together with the partitioning into reduced hierarchies. B: A comparison of the hybrid HEOM/QME method with exact HEOM result for the dimer model A with  $\beta\hbar\gamma_D = 0.25$ ,  $\beta\Delta\epsilon = 1$ ,  $\beta V = 0.1$ ,  $\beta\lambda_{CT} = 5$ ,  $\kappa = 1$ , and  $\beta\Delta E_{CT} = -6$  (left three columns) and for the dimer model B with  $\beta\hbar\gamma_D = 1.75$ ,  $\beta\Delta\epsilon = 1$ ,  $\beta V = 0.5$ ,  $\beta\lambda_{CT} = 5$ ,  $\kappa = 1$ , and  $\beta\Delta E_{CT} = -2$  (right three columns), with a range of values of  $\lambda_{LE}$  and  $J$ . The first/fourth columns show the total LE population dynamics, the second/fifth columns show the LE population difference relative to the total LE population, and the third/sixth columns show the real part of the LE coherence relative to the total LE population. The rows correspond to models with  $\beta J = 1, \beta\lambda_{LE} = 0.1$  (top),  $\beta J = 1, \beta\lambda_{LE} = 1$  (middle), and  $\beta J = 0.1, \beta\lambda_{LE} = 1$  (bottom). C: Convergence of the hybrid HEOM/QME results with respect to  $\Gamma_{c,ET}$  with parameters described in the text. The panels correspond to  $\kappa = 0$  (left) and  $\kappa = 1$  (right).

model is

$$\hat{H}_{LE,s} = \frac{\Delta\epsilon}{2} |LE_1\rangle\langle LE_1| - \frac{\Delta\epsilon}{2} |LE_2\rangle\langle LE_2| + J(|LE_1\rangle\langle LE_2| + |LE_2\rangle\langle LE_1|) \quad (60)$$

and the CT state Hamiltonian is taken to be  $\hat{H}_{CT,s} = (\Delta E_{CT} + \lambda_{CT}) |CT\rangle\langle CT|$  and the CT bath shift operator is taken as  $\Delta\hat{V}_{CT}^{bcr} = \hat{B}_{CT}$ , where  $\hat{B}_{CT}$  is a harmonic bath displacement

operator. The LE baths and the  $b_{CT}$  bath, are taken to have Debye spectral densities,<sup>11</sup>

$$\mathcal{J}_j(\omega) = \frac{\lambda_j}{2} \frac{\gamma_D \omega}{\gamma_D^2 + \omega^2} \quad (61)$$

where  $j = LE_1, LE_2$  or CT labels the bath. In this model we set  $\lambda_{LE_1} = \lambda_{LE_2} = \lambda_{LE}$  and only the  $LE_2$  state is coupled to the CT state with a coupling coefficient  $V_{LE_2,CT} = V$ . The correlation



coefficients  $\kappa_{LE_n}^{CT}$  describing the correlation between the CT state energy gap and the LE state energy gaps are taken to be  $\kappa_{LE_1}^{CT} = 0$  and  $\kappa_{LE_2}^{CT} = \kappa$ . The structure of the coupling between states and the partitioning into different HEOM/QME hierarchies,  $|\sigma_A(t)\rangle$ , is illustrated in Fig. 3 A.

The HEOM/QME calculations were performed with the adaptive short iterative Arnoldi integrator described in the SI of Ref. 73, with a Krylov subspace dimension of  $k = 9$ , and an error tolerance parameter of  $\epsilon = 10^{-12}$ . The hierarchy was truncated using the frequency cut-off criterion, with ADOs with  $\gamma_n > \Gamma_c = 10\gamma_D$  excluded from the hierarchy. The same cut-off scheme was used to truncate  $\tilde{V}$  in evaluating the electron transfer kernel, but with a looser choice of cut-off parameter  $\Gamma_{c,ET} = 2.5\gamma_D$ , so overall couplings between only 6 of the 55 ADOs were accounted for in evaluating  $\mathcal{R}_{AB}^{ET}$ . The HEOM was closed using the termination scheme and low temperature correction described in Ref. 73.

The exact HEOM calculations on the dimer model were also performed using the adaptive short iterative Arnoldi integrator with  $k = 9$  and  $\epsilon = 10^{-11}$ . The problem was simplified by reducing the number of baths from three to two as described in Appendix B – this greatly reduced the number of ADOs needed in the exact calculations. The hierarchy was truncated using a reorganization energy weighted frequency cut-off scheme, wherein ADOs with a weight  $w_n = \sum_{jk} v_{jk} n_{jk} / \lambda_j > \tilde{L}_c$  are excluded from the hierarchy, with  $\tilde{L}_c = 20$ . This scheme accounts for the fact that the hierarchy needs to be deeper for the modes with of larger reorganization energy baths, because coupling coefficients down the hierarchy scale as  $a_{jk} \propto \sqrt{\lambda_j}$ . This more efficiently truncates the HEOM than other schemes, such as the frequency cut-off scheme<sup>20</sup> or the  $L, M$  cut-off scheme.<sup>68</sup>

As a first example of the HEOM/QME method, we performed simulations for the dimer model with  $\beta\hbar\gamma_D = 0.25$ ,  $\beta\Delta\epsilon = 1$ ,  $\beta V = 0.1$ ,  $\beta\lambda_{CT} = 5$ ,  $\kappa = 1$ , and  $\beta\Delta E_{CT} = -6$  (labelled model A in Fig. 3 B), with a range of values of  $\lambda_{LE}$  and  $J$ . The initial condition was set to  $\hat{\sigma}_{LE}(0) = |\text{LE}_1\rangle\langle\text{LE}_1|$  and  $\hat{\sigma}_{CT}(0) = 0$ . We look at three regimes of the exciton dynamics: the damped coherent transport regime ( $\beta\lambda_{LE} = 0.1$  and  $\beta J = 1$ ), the vibrationally assisted transport regime ( $\beta\lambda_{LE} = 1$  and  $\beta J = 1$ ), and the incoherent Förster transport regime ( $\beta\lambda_{LE} = 0.1$  and  $\beta J = 0.1$ ). These model parameters are chosen to be typical of coupled LE and CT states in light harvesting complexes such as the Chl*a* dimer coupled to lutein in Fig. 1.<sup>21</sup>

In Fig. 3 B we compare the exact simulated dynamics to the hybrid HEOM/QME dynamics, looking at three observables: the total LE state population,  $p_{LE}(t)$ , the relative population difference between the LE states,  $(p_{LE_1}(t) - p_{LE_2}(t))/p_{LE}(t)$ , and the relative LE coherence, defined as  $2 \text{Re}[\langle\text{LE}_1|\hat{\sigma}_{LE,s}(t)|\text{LE}_2\rangle]/p_{LE}(t)$ . We see that in this example the hybrid HEOM/QME method performs excellently in the three regimes of exciton dynamics, with only small deviations in the long time limits of the relative LE population differences and coherences. In particular the time scale of decay of the LE population is captured very well by the hybrid method for all three models.

In a second more challenging test for the hybrid method,

we performed simulations for the same dimer model with  $\beta\hbar\gamma_D = 1.75$ ,  $\beta\Delta\epsilon = 1$ ,  $\beta V = 0.5$ ,  $\beta\lambda_{CT} = 5$ ,  $\kappa = 1$ , and  $\beta\Delta E_{CT} = -2$  (labelled model B in Fig. 3 B). In this example the coupling between the CT and the LE manifold is much larger, the free energy of CT state is higher, so back reaction effects are more significant. Furthermore the characteristic bath frequency is comparable now to the LE system frequencies, leading to significant non-Markovian effects in the LE dynamics, and the ET rate from the LE manifold to the CT state is closer to frequencies of the exciton dynamics. However in Fig. 3 A we see that the hybrid method still performs well in all regimes of exciton dynamics, with only small errors in the decay of the total LE population. The errors in the population dynamics can likely be attributed to the increased importance of CT-LE coherence in this example, which is treated with a perturbative-Markovian approximation with the hybrid method. Within high temperature perturbation theory, the steady-state average CT-LE coherence scales roughly as  $V/\lambda_{CT} = 0.1$ , which is five times larger in this set of models compared to the previous ones with  $V/\lambda_{CT} = 0.02$ , so it is not unexpected that the rate of ET is not captured quite as well in these more challenging models.

As a final example, we examine the convergence of the LE population dynamics with respect to the cut-off parameter  $\Gamma_{c,ET}$ , for two values of  $\kappa = 0$  and  $\kappa = 1$ . When  $\kappa = 1$ , there is no contribution from the  $b_{LE_2}$  bath to the free energy change or reorganization energy of the charge transfer process, however when  $\kappa = 0$  the  $b_{LE_2}$  reorganizes in the  $LE_2 \rightarrow CT$  transfer, which means when  $\kappa = 0$  this bath has a significant contribution to the free energy change and reorganization energy of the  $LE_2 \rightarrow CT$  process. In these simulations, we set  $\Gamma_c = 7\gamma_D$  and we examine the population dynamics for the  $\beta\lambda_{LE} = 1$ ,  $\beta J = 1$  with model parameters the same as in dimer model A (as in Fig. 3 B). In Fig. 3 C we show the population dynamics for various  $\Gamma_{c,ET}$  values for  $\kappa = 0$  and  $\kappa = 1$ . We see that convergence is much faster in the  $\kappa = 1$  case, where the LE bath does not contribute to the reorganization energy or free energy change of the  $LE \rightarrow CT$  process, so only the LE system energies need to be accounted for in the kernel to obtain accurate results. Conversely, when  $\kappa = 0$  there is a significant contribution to the reorganization energy and free energy change from the LE bath (roughly 20%) and therefore the LE bath response has to be accounted for in more detail in the ET kernel to obtain accurate results.

## V. LHCII

Having established the accuracy of the hybrid HEOM/QME method on a range of dimer models, we turn to a more complex problem, charge transfer energy quenching in LHCII. LHCII is an important light-harvesting complex in plants, which absorbs light energy and transports it to reaction centers.<sup>1</sup> It is also known to play a role in non-photochemical quenching in plants, and one mechanism for excitation energy quenching in the complex is electron transfer from the carotenoid lutein to excited chlorophyll-*a* molecules.<sup>6,8,62,74</sup> The resulting  $\text{Chl}a^{\bullet-}\text{Lut}^{\bullet+}$  pairs recombines to the ground state of the sys-

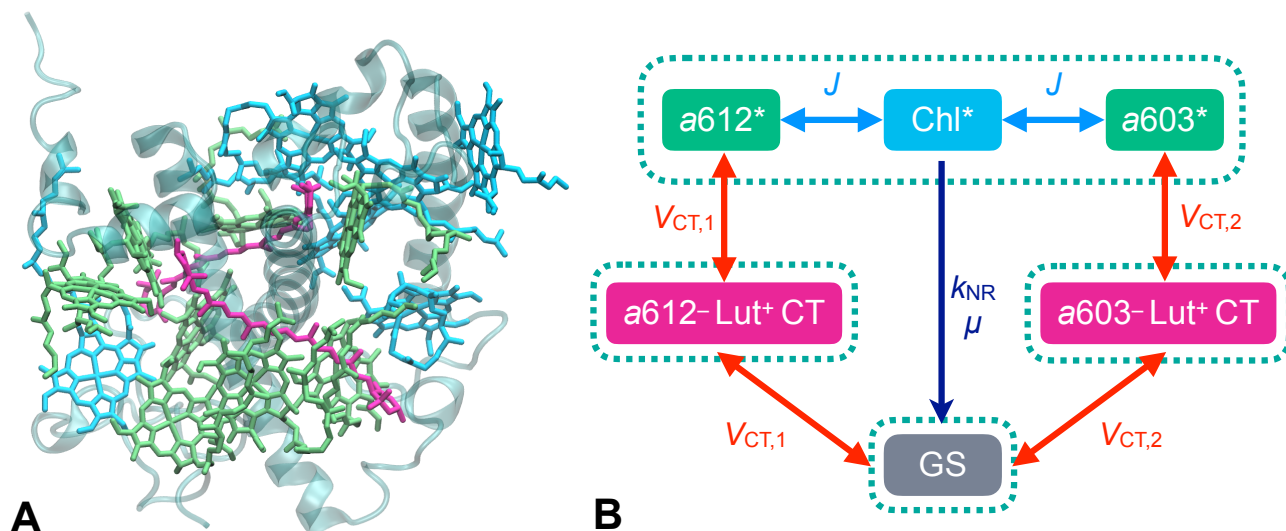


FIG. 4. A: The structure of the LHCII monomer (PDB 1RWT chain C<sup>63</sup>) showing the chlorophyll A (green), chlorophyll B (light blue), and lutein (pink) molecules. B: A scheme of the electronic states and couplings used in this model. Couplings between states are represented by double-headed arrows, the single-headed arrow represents the radiative and non-radiative transfer processes, and the dashed lines represent the blocks of states treated with their own explicit hierarchies of ADOs  $|\sigma_A(t)\rangle$ .

tem, thereby quenching excitation energy as heat. In Ref. 62 Cupellini *et al.* parametrized the free energy change, reorganization energy and diabatic coupling for charge transfer from Lut1 to  $a612^*$  and Lut2 to  $a603^*$ , and from this they used Marcus theory and a simple kinetic model to estimate the excitation lifetime of chlorophyll in LHCII. This model treated the coupled  $\text{Chla}^*$  and  $\text{Chlb}^*$  dynamics with a simple kinetic model, where EET between the  $a612^*$  and  $a603^*$  states and the pool of  $\text{Chla}^*$  states is modelled as a simple first order rate process. This treatment ignores many of the details of EET in LHCII, such as the strong coupling between the  $a612^*$  and  $a611^*$  states, and the  $a603^*$  and  $a602^*$  states, which leads to exciton formation.

### A. Model details

In order to go beyond a simple kinetic treatment of excitation energy transfer and CT quenching in LHCII, we have modeled the coupled exciton and charge transfer dynamics of an LHCII monomer with the hybrid HEOM/QME method. This allows us to fully explore the effects of coupled exciton and charge transfer dynamics on the  $\text{Chl}^*$  lifetime. The monomer contains eight  $\text{Chla}$  and six  $\text{Chlb}$  molecules, excitations on which are all coupled, together with two lutein molecules (Lut1 and Lut2), as shown in Fig. 4 A. We partition the system into an LE space, two CT states and the GS as outlined in Fig. 4 B. We explore this system using two different LE Hamiltonians for LHCII, which have been parametrized using various spectroscopic data: the model of Müh *et al.* from Ref. 61 (henceforth referred to as model 1) and the model of Novoderezhkin *et al.* from Ref. 41 (henceforth referred to as model 2). These models differ subtly in the  $\text{Chla}^*$  and  $\text{Chlb}^*$  site energies and couplings, which is shown below to have a significant effect on the quench-

ing dynamics. The LE-environment coupling is treated with the HEOM approach, with a single Debye bath for each site, with a reorganization energy of  $220 \text{ cm}^{-1}$  and characteristic frequency,  $\gamma_{\text{D,Chl}^*}$ , of  $353.7 \text{ cm}^{-1}$ , as taken from Kreisbeck *et al.*'s study in Ref. 21. This model for the LE-environment coupling misses some small vibrational resonance effects in the  $\text{Chlb}^*$  to  $\text{Chla}^*$  energy transfer dynamics, but it accurately captures the important features of the excitation energy dynamics when compared with more complex structured environment models.<sup>21</sup>

In order to describe the charge transfer process we use the reorganization energies, charge transfer free energy changes, and diabatic couplings calculated by Cupellini *et al.* from QM/MM simulations. The reorganization energy for the  $b_{\text{CT}}$  bath for each charge recombination process to the GS is assumed to be the same as for the corresponding charge separation, which is a reasonable assumption if polarization of the environment and lutein reorganization are the dominant contributions to the total reorganization energy, and the free energy of the GS relative to the excited states is taken from the LE model Hamiltonians. Using these parameters, we assume the  $b_{\text{CT}}$  bath can be treated as harmonic, with a Debye spectral density with  $\gamma_{\text{D}} = 30 \text{ cm}^{-1}$ , which is representative of the response of the polarizable environment.<sup>75</sup> We have also explored how adding structure to this spectral density affects the quenching dynamics, as will be explained below. For the Lut1  $\rightarrow a612^*$  charge transfer and Lut2  $\rightarrow a603^*$  charge transfer we used the same diabatic coupling matrix elements as calculated by Cupellini *et al.*,<sup>62</sup> denoted  $V_{\text{CT}1}$  and  $V_{\text{CT}2}$  respectively. We use the same diabatic couplings for the recombination processes  $a612^- \rightarrow \text{Lut1}^+$  and  $a603^- \rightarrow \text{Lut2}^+$ , given that the donor-acceptor separation is the same for the charge separation and charge recombination steps, although a different  $\text{Chla}$  orbital is involved in the recombination process, so the couplings will

be different in reality. The full set of parameters and the LE state Hamiltonians are given in Appendix D.

The transition dipole moment operators for the LE system are calculated using the atomic positions from PDB 1RWT<sup>63</sup> for the Chla and Chlb molecules and assuming the transition dipole moment for each LE state,  $\mu_n$ , points in the direction from  $N_B$  to  $N_D$ .<sup>76</sup> The magnitude of the transition dipole moment operator is taken to be 4.0 Debye for Chla and 3.4 Debye for Chlb.<sup>23</sup> In modelling excitation relaxation in the LHCII monomer it is also necessary to incorporate direct internal conversion of the Chla\* and Chlb\* states. This was done by adding the following non-radiative transition operators to the HEOM/QME

$$\mathcal{R}_{LE,LE}^{NR} \hat{\sigma}_{LE,n}(t) = - \sum_{n=1}^{N_{LE}} \frac{k_{NR,n}}{2} \{ |LE_n\rangle\langle LE_n|, \hat{\sigma}_{LE,n}(t) \} \quad (62)$$

$$\mathcal{R}_{GS,LE}^{NR} \hat{\sigma}_{LE,n}(t) = \sum_{n=1}^{N_{LE}} k_{NR,n} |GS\rangle\langle LE_n| \hat{\sigma}_{LE,n}(t) |LE_n\rangle\langle GS| \quad (63)$$

and we set  $k_{NR,n} = 0.25 \text{ ns}^{-1}$ , in line with Cupellini *et al.*'s kinetic model.<sup>62</sup> A similar model has been used previously in quantum master equation based studies of the bacterial LHI/LHII system,<sup>76</sup> and a justification of this form of the non-radiative transition operator from the Nakajima-Zwanzig equation is given in Appendix C.

In all simulations with the hybrid HEOM/QME method we use an adaptive Short iterative Arnoldi integrator (as described in Ref. 73) with an error tolerance parameter of  $10^{-8}$ , and Krylov subspace dimension of 16. The Nakajima-Zwanzig low temperature and termination corrections described in Ref. 73 were also used in these simulations, and using this scheme the populations of Chla\*, Chlb\* and CT states were found to be converged with an HEOM frequency cut-off parameter of  $\Gamma_c = 3\gamma_{D,Chl^*}$ , using the Matsubara decomposition scheme for the correlation functions. The cut-off parameter for the ET kernels was set to  $\Gamma_{c,ET} = 2\gamma_{D,Chl^*}$  for the charge separation steps and  $\Gamma_{c,ET} = 0$  for the charge recombination steps. All simulations were run at a temperature of 300 K. These methods are all implemented in the freely available HEOM-lab code,<sup>77</sup> which was used to perform all simulations presented in this paper.

## B. Population dynamics

As a first application of the hybrid HEOM/QME method to LHCII charge transfer quenching, we have simulated the population dynamics for the Chla\*, Chlb\* and CT states for Model 1, with the initial condition set as an excitation completely localized on a612. The population dynamics are shown in Fig. 5. For this initial condition there is an early rapid transfer of population to the strongly coupled a611\* state, as an exciton is formed where the excitation is delocalized between the two Chla sites. This exciton formation is followed by slower excitation energy transfer to the other Chla\* and Chlb\* states,

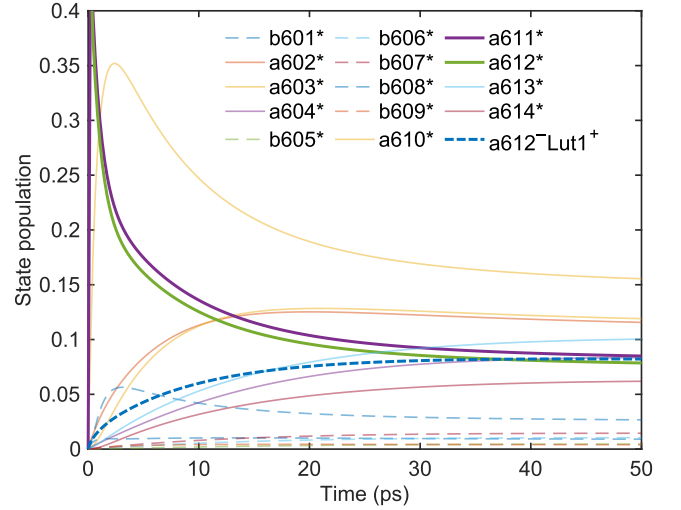


FIG. 5. Populations of the LE states and the  $a612^-Lut1^+$  state calculated with the hybrid HEOM/QME method for an initial excitation localized on a612, using the model 1 LE Hamiltonian.

as well as the  $a612^-Lut1^+$  state. Importantly, formation of the  $a612^-Lut1^+$  state from the exciton state happens on a comparable time-scale, roughly 10 ps, to energy redistribution between the Chla\* and Chlb\* states highlighting the need to treat both the CT and exciton dynamics simultaneously. We found that at least  $\Gamma_c = 3\gamma_{D,Chl^*}$  was needed to converge the population dynamics, with hierarchy termination corrections from Ref. 73, which corresponds to treating the exciton system-environment coupling up to sixth order in non-Markovian perturbation theory, with partial Markovian eighth order corrections. This illustrates the simple mixed Redfield-Förster theories would likely be insufficient for describing the population dynamics of this system, as has been demonstrated previously by Kreisbeck *et al.*<sup>21</sup> This calculation would be intractable with standard HEOM methods due to the very large reorganization energy associated with the charge transfer processes, but with the hybrid HEOM/QME method this calculation is runs in a few minutes on a single CPU.

In order to compare the kinetic model used by Cupellini *et al.* to our model including the full exciton dynamics, we have also simulated the population dynamics where population is evenly divided between the Chla\* states, with no initial coherences between sites. The total populations of the Chl\*, Chla\*, Chlb\*, and the populations of the CT states and GS are shown for both models in Fig. 6. In both models there is rapid equilibration between the Chla\* and Chlb\* states, occurring on a time scale of a few picoseconds, followed by population transfer to the CT states within ten picoseconds. The  $a612^-Lut1^+$  state is populated to a much greater extent than the  $a603^-Lut2^+$  state, because the latter lies nearly  $1000 \text{ cm}^{-1}$  above the Chla\* states, whereas the former is nearly degenerate with the Chla\* states. In model 1 we observe a greater extent of population transfer to the Chlb\* states and a lesser population of the  $a612^-Lut1^+$  state compared to model 2.

Interestingly, the overall decay of the Chl\* population is noticeably faster in model 2 compared to model 1. In order

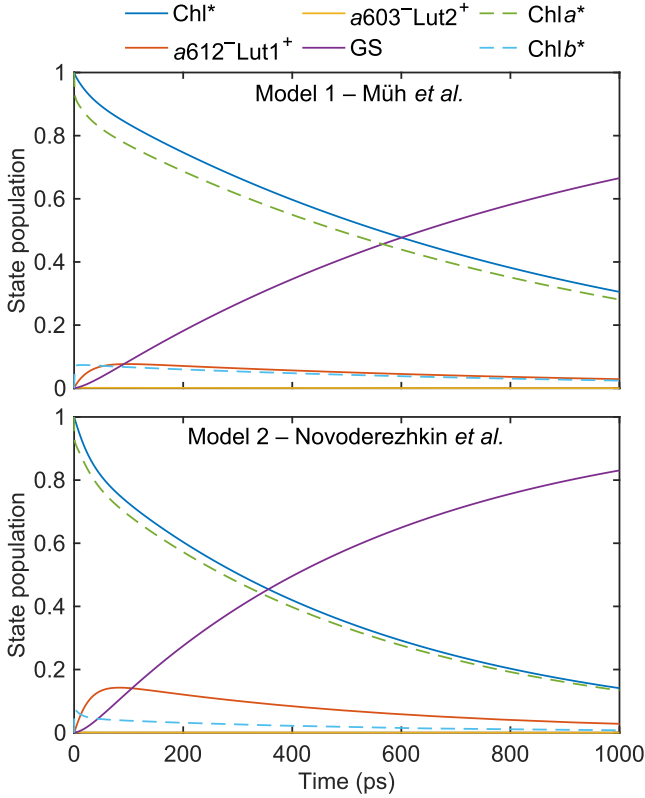


FIG. 6. Excited state population dynamics for LHCII with an initial excitation partitioned equally between all eight  $\text{Chl}a^*$  states with no coherences between these states, calculated with the hybrid HEOM/QME method. Results in the top panel use the model 1 LE Hamiltonian and results in the bottom panel use the model 2 LE Hamiltonian.

to quantify the excitation lifetime, we fit these population decay curves to a sum of three exponentials (constrained such that  $p_{\text{Chl}^*}(t=0) = 1$ ), and use this to calculate the integrated lifetime  $\tau_{\text{eff}} = \int_0^\infty p_{\text{Chl}^*}(t) dt$ . For model 1 we obtain  $\tau_{\text{eff}} = 0.83$  ns and for model 2 we find  $\tau_{\text{eff}} = 0.50$  ns. These lifetime estimates are both closer to the experimental value for the excitation lifetime, 2 ns for LHCII in a membrane, than Cupellini *et al.*'s kinetic model, which predicted a 0.3 ns integrated lifetime. This suggests the importance of treating the exciton dynamics explicitly in modeling charge transfer quenching in light-harvesting complexes. We suspect that a significant source of error in our model, compared to experiment, is the estimate for the diabatic coupling for the charge recombination steps, which affects the lifetime of the CT states, and therefore also strongly influences the CT quenching rate.

Part of the difference between Cupellini *et al.*'s kinetic model, and our model is that we correctly account for exciton formation in the excited state dynamics, which changes the rate of population transfer from the LE manifold to the CT states. This is because exciton formation modifies the effective coupling matrix element by  $\sim 1/\sqrt{2}$  for the charge transfer rate, since charge transfer occurs from the excitonic state  $|\psi\rangle \approx (1/\sqrt{2})(|a611^*\rangle - |a612^*\rangle)$  (although this picture is complicated by the LE bath reorganization, which reduces

the relative coherence between the  $a611^*$  and  $a612^*$  states to  $\sim 0.16$  for model 1 and  $\sim 0.20$  for model 2). Furthermore exciton formation lowers the free energy of the initial excitonic state by  $\sim 100 \text{ cm}^{-1}$  for both models. This means the effective free energy change for the formation of the  $a612^- \text{Lut}1^+$  is approximately  $0 \text{ cm}^{-1}$ , which is reflected in Fig. 5 where the  $a611^*$ ,  $a612^*$  and  $a612^- \text{Lut}1^+$  states all have approximately equal population by  $t = 50$  ps. This means the excitonic state is stabilized relative to the CT state and this decreases the steady state CT population, decreasing the rate of charge separation

The faster quenching in model 2 is primarily due to the larger steady-state population of the  $a612^- \text{Lut}1^+$  which provides the main channel for charge transfer quenching of the  $\text{Chl}^*$  excitations. The larger steady state population of the  $a612^- \text{Lut}1^+$  state can be explained by the differences between the excitonic structure of the two LHCII models. In model 1, the  $a611^- \text{a}612^-$  excitonic state is the third lowest energy state, lying more than  $k_B T$  above the lowest lying excitonic state, whereas in model 2 the  $a611^- \text{a}612^-$  excitonic state is the lowest energy state, with the next nearest excitonic state lying about  $0.5 k_B T$  above this. This means that in model 2 more of the  $\text{Chl}a^*$  excitations are funnelled into the excitonic state which couples to the quenching state, which leads to a greater extent of CT state formation, and faster  $\text{Chl}^*$  population decay. This illustrates the importance of the excitonic energy funnel in determining quenching efficiency.

### C. Role of the excitation energy funnel

In order to further explore the effects of the excitonic energy funnel on excitation quenching in LHCII, we have performed simulations on modified versions of the model 1 and model 2  $\text{Chl}^*$  Hamiltonians. For both models we introduced a shift to the site energies of all states in the LE manifold except the  $a611$  and  $a612$  states, such that the site energies are changed from  $E_n$  to  $E_n + \delta E$ . The energy of the  $a603^- \text{Lut}2^+$  charge transfer is shifted by the same amount. This effectively preserves the  $a611^- \text{a}612^-$  exciton state in the LE manifold, but just shifts its energy relative to the remaining excitonic states. Varying the shift from  $-500 \text{ cm}^{-1}$  to  $+500 \text{ cm}^{-1}$ , we have calculated the total  $\text{Chl}^*$  population decay and the integrated lifetime from the population dynamics to quantify the changes to the  $\text{Chl}^*$  excitation lifetime, as shown in Fig. 7.

We see that for modified versions of both model 1 and model 2, shifts in the  $\text{Chl}^*$  site energies can have a very large effect on the population dynamics and excitation lifetime. In particular for model 1 a change in shift from  $-200 \text{ cm}^{-1}$  to  $+200 \text{ cm}^{-1}$  can change the excitation lifetime by more than a factor of 2. These significant changes in excitation lifetime for modest shifts in the excitation energies suggest a potential mechanism for activation of non-photochemical quenching by changes in the energy funnel in light-harvesting complexes directing excitations towards quenching sites.

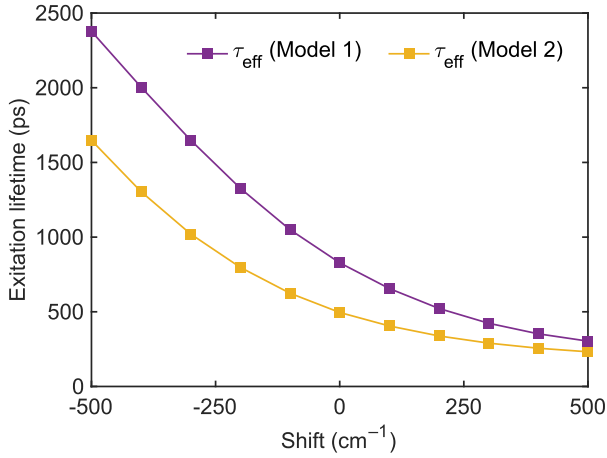


FIG. 7.  $\tau_{\text{eff}}$  and  $\tau_{\text{max}}$  for models 1 and 2 as a function of the local excitation energy shift, as described in the text.

#### D. Role of the charge transfer spectral density

We have examined the potential role of nuclear quantum effects in determining the charge transfer quenching lifetime. We modify the spectral density for the charge transfer processes to include an underdamped Brownian oscillator contribution,<sup>11</sup> where the new spectral density is

$$\mathcal{J}_{\text{CT}}(\omega) = (1 - \alpha)\mathcal{J}_{\text{D}}(\omega) + \alpha\mathcal{J}_{\text{BO}}(\omega) \quad (64)$$

$$\mathcal{J}_{\text{BO}}(\omega) = \frac{\lambda}{2} \frac{\gamma\Omega^2\omega}{(\omega^2 - \Omega^2)^2 + \gamma^2\omega^2} \quad (65)$$

where the first portion is a Debye spectral density with  $\omega_{\text{D}} = 30 \text{ cm}^{-1}$ , which represents the low frequency environment contribution, and  $\mathcal{J}_{\text{BO}}(\omega)$  models the high frequency contribution from C=C stretches in the lutein molecules.<sup>78</sup> In what follows we have set  $\Omega = 1500 \text{ cm}^{-1}$  and  $\gamma = 50 \text{ cm}^{-1}$ , and we keep the total reorganization energy for each charge transfer process fixed at the values determined by Cupellini *et al.* We have varied the  $\alpha$  parameter, which controls the spectral distribution of the reorganization energy, between 0 and 0.5 for the model 1 exciton Hamiltonian, and for each value of  $\alpha$  we have simulated the population dynamics and calculated  $\tau_{\text{eff}}$  and  $\tau_{\text{max}}$ , again from an initial condition where all Chl $a^*$  states are equally populated with no coherences.

The calculated total Chl $a^*$  and  $a612^- \text{Lut}1^+$  population dynamics are shown in the top panels of Fig. 8. We see that increasing the contribution to the charge transfer spectral density from the underdamped, high frequency Brownian oscillator decreases the lifetime of the Chl $a^*$  excitations. The increased Brownian oscillator contribution increases the extent of nuclear quantum tunneling, which increases both the rate of charge separation and charge recombination. The effect of increasing the rates of both processes can be seen more clearly in the  $a612^- \text{Lut}1^+$  population dynamics. At short times, as  $\alpha$  increases, the rate of population transfer from the Chl $a^*$  manifold to the  $a612^- \text{Lut}1^+$  increases due to an increasing charge separation rate, which transiently increases the quenching rate. At longer times, when the Chl $a^*$  states and CT states have reached

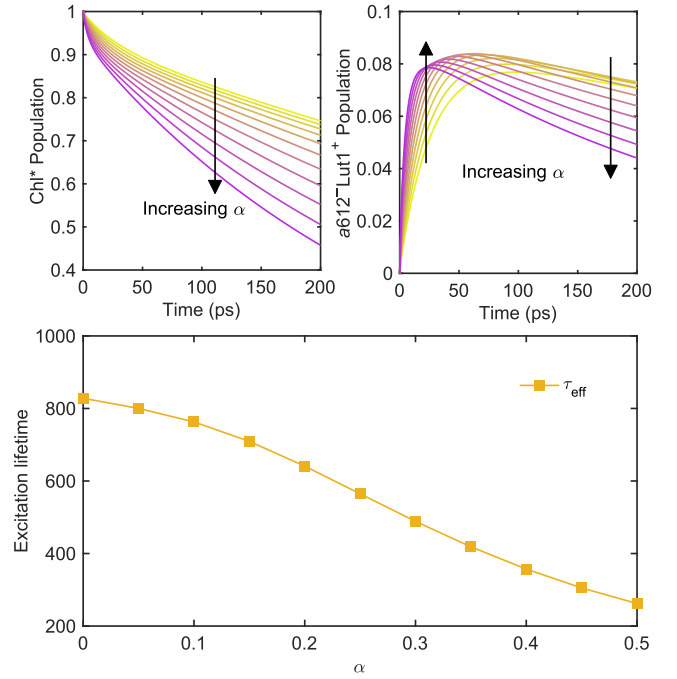


FIG. 8. Top left: Chl $a^*$  population dynamics varying  $\alpha$  from 0 (yellow) to 0.5 (purple). Top right:  $a612^- \text{Lut}1^+$  population dynamics varying  $\alpha$  (same color scheme as top left). Bottom: excitation lifetime as a function of  $\alpha$ . All calculations use the model 1 LE Hamiltonian with equally populated Chl $a^*$  states with no coherences as the initial condition.

a steady state, increasing  $\alpha$  increases the rate of decay of the  $a612^- \text{Lut}1^+$  state, which arises due to the increased charge recombination rate with increasing  $\alpha$ .

## VI. DISCUSSION

Using the hybrid HEOM/QME method developed in this paper we have been able to explore the charge transfer quenching dynamics in a LHCII monomer. Using previously parametrized models of excitation energy transfer and electron transfer in the LHCII pigment-protein complex, together with some physically motivated assumptions, we can obtain estimates of the excitation lifetime closer to experimental values than those obtained using simple kinetic models.<sup>62</sup> The lifetime estimate however depends strongly on the model of local excitation energies and couplings used to describe the excitation energy transfer preceding charge transfer quenching. This may have interesting implications for the understanding of non-photochemical quenching processes in light harvesting complexes. It is generally assumed that non-photochemical quenching is activated by conformational changes, induced by pH changes or chemical modifications of the protein or bound carotenoids, in protein-pigment complexes moving quenchers into positions where they can efficiently couple to chromophores,<sup>6,7,74,79-82</sup> thereby increasing the rate of charge transfer quenching and/or excitation energy transfer quenching. The work here highlights the potential role of the excita-

tion energy funnel in CT quenching, and we suggest that non-photochemical quenching could also be activated by changes in the site energies and couplings within the chromophore excited state manifold that funnel excitations towards quenching sites. These energy and coupling shifts could also be induced by conformational changes in the protein-pigment complex, and could occur simultaneously with the conformational changes that move quenchers closer to chromophores. In this way, the energy funnelling mechanism could work cooperatively with quenching activation by movement of quenchers. Interestingly it has recently been found in one computational study that pH changes, which are believed to play a role in activating non-photochemical quenching, can create modest shifts in the Chl excitation energies in LHCII.<sup>83</sup>

Our exploration of the charge transfer spectral density has also highlighted the importance of understanding all details of charge transfer processes in light harvesting complexes, including the details of recombination processes and nuclear quantum effects. One particularly important factor for predicting charge transfer quenching rates is the rate of charge recombination from the CT state back to the electronic ground state of the system, which is strongly dependent on nuclear quantum effects as well as the energetics of charge recombination and the diabatic coupling strength. This is because the reverse electron transfer is often deep in the Marcus inverted regime, for example in LHCII the Lut-Chl $a$  recombination processes have a free energy change of  $-\Delta G \approx 3\lambda$ , where nuclear tunnelling effects play a decisive role in determining electron transfer rates.<sup>84</sup> Although in our study of LHCII we have assumed that the electron transfers can be treated with a spin-boson mapping,<sup>27</sup> the theory developed here does not rely on this assumption. The correlation functions needed to evaluate the ET kernels,  $G_{AB}^C(t)$ , can be evaluated using various approximations including anharmonicity in the potential energy surfaces.<sup>50,85–89</sup> For example  $G_{AB}^C(t)$  could be evaluated classically,<sup>50</sup> or using analytic continuation together with path integral methods to incorporate anharmonic nuclear quantum effects.<sup>88</sup>

## VII. CONCLUDING REMARKS

In this paper we have outlined how to rigorously combine the hierarchical equations of motion method with quantum master equations in both the strong system-bath coupling and weak system-bath coupling limits, to model simultaneous excitation energy transfer and charge transfer in protein-pigment complexes. The hybrid HEOM/QME approach is based the application of Zwanzig projection, to derive a system of equation for a hierarchy of auxiliary density operators for the various electronic state manifolds. This method has been tested against numerically exact results for an excitonic dimer coupled to a charge transfer state, where it was found to yield accurate population and coherence dynamics across a range of excitation energy transfer regimes. We then applied the method to study charge transfer quenching in LHCII - a process suspected to play an important role in photoprotection in plants.

Using the hybrid HEOM/QME approach we have been able

to study the interplay of excitation energy transfer and charge transfer quenching in a realistic model of LHCII. Our results highlight the importance of the excitation energy funnel in determining quenching efficiency in protein-pigment complexes, as well as the role of the CT state recombination rate when back electron transfer to reform LE states from CT states occurs at an appreciable rate, as is the case in LHCII. We expect that the energy funnel mechanism could play a role in activation of non-photochemical quenching in many systems, and that it could occur co-operatively with other NPQ activation mechanisms.

The parameters needed in the hybrid HEOM/QME model can all be obtained using well-established methods, for example exciton Hamiltonians can be fit based on spectroscopic data,<sup>41,61</sup> or using QM/MM simulations of protein-pigment complexes.<sup>90</sup> Likewise electron transfer model parameters can be obtained using molecular dynamics simulations.<sup>27,87</sup> By combining existing computational tools with the hybrid HEOM/QME method, currently implemented in the freely available Matlab code HEOM-lab,<sup>77</sup> it may be possible to shed light on the precise mechanisms that produce non-photochemical quenching in photosynthetic organisms,<sup>6</sup> for example how chemical modifications of carotenoids in the xanthophyll cycle activates NPQ in LHCII and related proteins like LHCX1.<sup>7,79</sup> For this reason we anticipate the method will become a useful tool in studying non-photochemical quenching and reaction center processes in photosynthetic systems.

## ACKNOWLEDGEMENTS

T. P. F and D.T.L. were supported by the U.S. Department of Energy, Office of Science, Basic Energy Sciences, CPIMS Program Early Career Research Program under Award DE-FOA0002019.

## Appendix A: The radiative decay term

We evaluate the radiative coupling term in the hybrid HEOM/QME in much the same way as the ET coupling term. Here we assume that only the LE states and the GS are connected by the dipole moment operator, which means we only have to evaluate  $\mathcal{R}_{GS,LE}^R$  and  $\mathcal{R}_{LE,LE}^R$ . Starting with  $\mathcal{R}_{GS,LE}^R$  we can insert the dipole coupling term into the second order kernel and directly evaluate the radiative coupling term as

$$\begin{aligned} \mathcal{R}_{GS,LE}^R &= \frac{1}{2\hbar\mathcal{V}_0\epsilon_0} \sum_{k,p} \int_0^\infty dt \omega_k \\ &\times \left( \mathcal{L}_{kp}^L e^{\mathcal{L}_0, st} \mathcal{L}_{kp}^R \left\langle a_{kp}(0) a_{kp}^\dagger(t) \right\rangle_{\text{bEM}} \right. \\ &\left. + \mathcal{L}_{kp}^R e^{\mathcal{L}_0, st} \mathcal{L}_{kp}^L \left\langle a_{kp}(0) a_{kp}^\dagger(t) \right\rangle_{\text{bEM}}^* \right) \end{aligned} \quad (\text{A1})$$

where we have assumed that we can approximate  $\mathcal{L}_0 + \mathcal{V} \approx \mathcal{L}_{0,s}$  in evaluating this term. The operators  $\mathcal{L}_{kP}^{L/R}$  are given by

$$\mathcal{L}_{kP}^L \hat{\sigma} = i\hat{\Pi}_{\text{GS}}(\hat{\boldsymbol{\mu}} \cdot \mathbf{e}_{kP})\hat{\Pi}_{\text{LE}}\hat{\sigma} \quad (\text{A2})$$

$$\mathcal{L}_{kP}^R \hat{\sigma} = -i\hat{\sigma}\hat{\Pi}_{\text{LE}}(\hat{\boldsymbol{\mu}} \cdot \mathbf{e}_{kP})\hat{\Pi}_{\text{GS}}, \quad (\text{A3})$$

and the EM field operator correlation function can be evaluated as

$$\left\langle a_{kP}(0)a_{kP}^\dagger(t) \right\rangle_{\text{bEM}} = \text{Tr}_{\text{bEM}} [\hat{a}_{kP}(0)\hat{a}_{kP}^\dagger(t)\hat{\rho}_{\text{bEM}}] = e^{i\omega_k t}. \quad (\text{A4})$$

In the limit of a large cavity volume for the EM field  $\mathcal{V}_0$ , we can replace the sum over cavity modes  $\mathbf{k}$  with an integral as

$$\frac{1}{\mathcal{V}_0} \sum_{\mathbf{k}} \rightarrow \frac{1}{(2\pi)^3} \int d\mathbf{k}. \quad (\text{A5})$$

After evaluating the angular part of the integral we arrive at

$$\begin{aligned} \mathcal{R}_{\text{GS,LE}}^R &= \frac{1}{6\hbar\epsilon_0\pi^2} \sum_{\alpha=x,y,z} \int_0^\infty dk \int_0^\infty dt c_0 k^3 \\ &\times \left( \mathcal{L}_\alpha^L e^{\mathcal{L}_{0,s}^{\text{LE,GS}} t} \mathcal{L}_\alpha^R e^{ic_0 k t} + \mathcal{L}_\alpha^R e^{\mathcal{L}_{0,s}^{\text{GS,LE}} t} \mathcal{L}_\alpha^L e^{-ic_0 k t} \right), \end{aligned} \quad (\text{A6})$$

then we insert the spectral resolution of  $\mathcal{L}_{0,s}$  acting on the GS-LE coherences ( $|\text{GS}\rangle\langle\text{LE}_n|$ ), and note that all the eigenvalues of this operator are purely imaginary, so we can write these as  $\mathcal{L}_{0,s}^{\text{GS,LE}} = \mathcal{S}_{\text{GS,LE}}^{0,s} (i\Omega_{\text{GS,LE}}) (\mathcal{S}_{\text{GS,LE}}^{0,s})^{-1}$  and  $\mathcal{L}_{0,s}^{\text{LE,GS}} = \mathcal{S}_{\text{LE,GS}}^{0,s} (-i\Omega_{\text{LE,GS}}) (\mathcal{S}_{\text{LE,GS}}^{0,s})^{-1}$ , where  $\Omega_{\text{GS,LE}}$  and  $\Omega_{\text{LE,GS}}$  are diagonal matrices with real positive-valued entries. We then evaluate the time integral, noting the imaginary part vanishes, and change variables in the  $k$  integral to  $\omega = c_0 k$  to give

$$\begin{aligned} \mathcal{R}_{\text{GS,LE}}^R &= \frac{1}{6\hbar\epsilon_0 c_0^3 \pi} \sum_{\alpha=x,y,z} \int_0^\infty d\omega \omega^3 \\ &\times \left( \mathcal{L}_\alpha^L \mathcal{S}_{\text{LE,GS}}^{0,s} \delta(\Omega_{\text{LE,GS}} - \omega) (\mathcal{S}_{\text{LE,GS}}^{0,s})^{-1} \mathcal{L}_\alpha^R \right. \\ &\left. + \mathcal{L}_\alpha^R \mathcal{S}_{\text{GS,LE}}^{0,s} \delta(\Omega_{\text{GS,LE}} - \omega) (\mathcal{S}_{\text{GS,LE}}^{0,s})^{-1} \mathcal{L}_\alpha^L \right). \end{aligned} \quad (\text{A7})$$

Integrating over  $\omega$  then yields in the expressions given in Eq. (58). These steps can be repeated for  $\mathcal{R}_{\text{LE,LE}}^R$  to obtain Eq.(59), where additionally we discard imaginary terms (which correspond to Lamb shifts).

## Appendix B: Simplification of the dimer model baths

In this appendix we describe how the three-bath model for the dimer-CT model can be reduced to a two bath model to speed up exact HEOM calculations. Suppose we have a system coupled to a set of baths,  $j = 1, \dots, N$ , with identical frequency distributions, but different reorganization energies, i.e.  $\mathcal{J}_j(\omega) = \eta_j \mathcal{J}_0(\omega)$  with  $\eta_j = \lambda_j/\lambda_0$ , as in the dimer CT

model considered here. We can write the coupling term for bath modes with frequency  $\omega_{j\alpha} = \omega_{0\alpha}$  as

$$\hat{H}_{\text{sb},\alpha} = c_\alpha \hat{\mathbf{q}}_\alpha \cdot \boldsymbol{\eta}^{1/2} \hat{\mathbf{V}} \quad (\text{B1})$$

where  $c_\alpha = c_{0\alpha}$ ,  $[\hat{\mathbf{q}}_\alpha]_j = \hat{q}_{j\alpha}$ ,  $[\hat{\mathbf{V}}]_j = \hat{V}_j$ , and  $\boldsymbol{\eta}$  is a diagonal matrix of the values of  $\eta_j$ . We can insert an orthogonal matrix  $\mathbf{S}$ , to re-write this as

$$\hat{H}_{\text{sb},\alpha} = c_\alpha \hat{\mathbf{q}}_\alpha^\top \mathbf{S}^\top \boldsymbol{\eta}^{1/2} \hat{\mathbf{V}} = c_\alpha \hat{\tilde{\mathbf{q}}} \cdot \hat{\tilde{\mathbf{V}}}. \quad (\text{B2})$$

We can then re-write the Hamiltonian in terms of a new set of uncorrelated baths with mode displacements  $\hat{q}_{j\alpha}$ , and coupling operators  $\hat{V}_j$ . If we choose  $\mathbf{S}$  such that one of the new system bath coupling operators is just proportional to the identity operator  $\hat{V}_1 \propto \hat{1}$ , then we eliminate coupling between one of the baths and the system, and therefore reduce the complexity of the problem. For  $\kappa = 1$  we can find such a transformation as follows. First we write  $\boldsymbol{\eta}^{1/2} \hat{\mathbf{V}}$  as

$$\boldsymbol{\eta}^{1/2} \hat{\mathbf{V}} = \begin{pmatrix} |\text{LE}_1\rangle\langle\text{LE}_1| \\ |\text{LE}_2\rangle\langle\text{LE}_2| + \kappa |\text{CT}\rangle\langle\text{CT}| \\ \sqrt{\eta} |\text{CT}\rangle\langle\text{CT}| \end{pmatrix} \quad (\text{B3})$$

where  $\lambda_0 = \lambda_{\text{LE}}$  and  $\eta = \sqrt{\lambda_{\text{CT}}/\lambda_{\text{LE}}}$ . We then set  $\mathbf{S}$  as

$$\mathbf{S} = \begin{pmatrix} \frac{1}{\sqrt{2}} & \frac{1}{\sqrt{2}} & 0 \\ \frac{1}{\sqrt{2}} & -\frac{1}{\sqrt{2}} & 0 \\ 0 & 0 & 1 \end{pmatrix} \quad (\text{B4})$$

which gives  $\hat{\tilde{\mathbf{V}}}$  as

$$\hat{\tilde{\mathbf{V}}} = \begin{pmatrix} \frac{1}{\sqrt{2}} \hat{1} \\ \frac{1}{\sqrt{2}} (|\text{LE}_1\rangle\langle\text{LE}_1| - |\text{LE}_2\rangle\langle\text{LE}_2| - |\text{CT}\rangle\langle\text{CT}|) \\ \sqrt{\eta} |\text{CT}\rangle\langle\text{CT}| \end{pmatrix}. \quad (\text{B5})$$

We see that the system coupling operator for the new bath 1 is proportional to an identity operator, so coupling to this bath does not affect the system dynamics and it can be eliminated.

For the  $\kappa = 0$  case we set

$$\mathbf{S} = \begin{pmatrix} \frac{1}{\sqrt{2+\eta^{-1}}} & \frac{1}{\sqrt{2+\eta^{-1}}} & \frac{1}{\sqrt{\eta(2+\eta^{-1})}} \\ \frac{1}{\sqrt{2}} & -\frac{1}{\sqrt{2}} & 0 \\ -\frac{1}{\sqrt{2+4\eta}} & -\frac{1}{\sqrt{2+4\eta}} & \frac{2\sqrt{\eta}}{\sqrt{2+4\eta}} \end{pmatrix} \quad (\text{B6})$$

which gives  $\hat{\tilde{\mathbf{V}}}$  as

$$\hat{\tilde{\mathbf{V}}} = \begin{pmatrix} \frac{1}{\sqrt{2+\eta^{-1}}} \hat{1} \\ \frac{1}{\sqrt{2}} (|\text{LE}_1\rangle\langle\text{LE}_1| - |\text{LE}_2\rangle\langle\text{LE}_2|) \\ \frac{1}{\sqrt{2+4\eta}} (2\eta |\text{CT}\rangle\langle\text{CT}| - |\text{LE}_1\rangle\langle\text{LE}_1| - |\text{LE}_2\rangle\langle\text{LE}_2|) \end{pmatrix}. \quad (\text{B7})$$

Again bath 1 can be eliminated because its coupling operator is proportional to an identity operator. We note that only the top row of  $\mathbf{S}$  is uniquely defined for any  $\kappa$ , by requiring that

$\hat{V}_1 \propto \hat{1}$ , and the choice for the other rows, and other coupling operators, is not unique.

Finally we note that we can scale the reorganization energy of a given bath by  $\alpha$  if we also scale the corresponding coupling operator by  $1/\sqrt{\alpha}$ , because the coupling coefficients are proportional to  $\sqrt{\lambda_j}$ ,  $c_{j\alpha} \propto \sqrt{\lambda_j}$ , without changing the Hamiltonian. The choice does not affect the exact dynamics, but it does affect how the hierarchy is truncated with our reorganization energy weighted cut-off scheme. For the calculations we set  $\lambda_2 = \lambda_{LE}$  and  $\lambda_3 = \lambda_{CT}$ , which means the coupling operator  $\hat{V}_3$  given above scaled down by  $1/\sqrt{\eta}$ .

### Appendix C: The internal conversion term

In this appendix we present a brief justification of the Lindblad form for the internal conversion term used to model direct non-radiative transitions from the Chl\* states to the ground state in LHCII. The argument is essentially the same as that used to derive the radiative and ET coupling Hamiltonians. We start by assuming that the internal conversion coupling is described by a Hamiltonian of the form

$$\hat{H}_{LE,GS} = \sum_{n=1}^{N_{LE}} \left( \hat{X}_n |GS\rangle\langle LE_n| + \hat{X}_n^\dagger |LE_n\rangle\langle GS| \right) \quad (C1)$$

where we assume the  $\hat{X}_n$  operator acts on degrees of freedom other than the  $b_{LE}$  degrees of freedom, and we also assume that these operators commute at all times. We also assume that the thermal average of  $\hat{X}_n$  is zero. The non-adiabatic coupling between the LE states and the ground state depends primarily on local vibrational modes of the chromophore, so it is reasonable to assume that these operators commute.

We can now evaluate the second order Markovian Nakajima-Zwanzig relaxation operator for internal conversion with the projection operator given in main text. We will further approximate the reference Liouvillian as  $\mathcal{L}_0 + \mathcal{V} \approx -\frac{i}{\hbar} [\hat{\Pi}_{LE} \bar{E}_{LE}, \cdot] \otimes$

$\mathcal{I}_{ado}$ , where  $\bar{E}_{LE}$  is the average LE state energy, an approximation that is justified because the mean energy difference between the LE states and the ground-state is much larger than energy differences within the LE manifold. From this it is straightforward to obtain the relaxation superoperator as

$$\mathcal{R}_{LE,LE}^{NR} \hat{\sigma} = \sum_{n=1}^{N_{LE}} \int_0^\infty dt \left( \langle X_n^\dagger(t) X_n(0) \rangle_b e^{i\bar{E}_{LE}t/\hbar} |LE_n\rangle\langle LE_n| \hat{\sigma} + \langle X_n^\dagger(t) X_n(0) \rangle_b^* e^{-i\bar{E}_{LE}t/\hbar} \hat{\sigma} |LE_n\rangle\langle LE_n| \right). \quad (C2)$$

Ignoring Lamb shift terms that originate from the imaginary parts of the  $\langle X_n^\dagger(t) X_n(0) \rangle_b$  correlation functions, this reduces to

$$\mathcal{R}_{LE,LE}^{NR} \hat{\sigma} = - \sum_{n=1}^{N_{LE}} \frac{k_{NR,n}}{2} \{ |LE_n\rangle\langle LE_n|, \hat{\sigma} \} \quad (C3)$$

where  $k_{NR,n}$  is the non-radiative decay rate for internal conversion of state  $LE_n$ . The corresponding term in the equation of motion for  $\hat{\sigma}_{GS,n}(t)$  is

$$\mathcal{R}_{GS,LE}^{NR} \hat{\sigma} = \sum_{n=1}^{N_{LE}} k_{NR,n} |GS\rangle\langle LE_n| \hat{\sigma} |LE_n\rangle\langle GS|. \quad (C4)$$

The reverse internal conversion rate is related to the forward rate by  $k_{NR,n}^{back} = e^{-\beta \bar{E}_{LE}} k_{NR,n}$ , but because  $\beta \bar{E}_{LE}$  is typically very large, we can safely ignore the back reaction terms.

### Appendix D: Additional details of the LHCII models

In this appendix we list the model parameters used in our simulations of the LHCII monomer. Firstly the LE system Hamiltonians for the two LHCII models are

$$\mathbf{H}_{LE,s} = (E_{LE} + \lambda_{Chl^*}) \mathbf{1} + \begin{pmatrix} 635 & 36 & -5 & -3 & 1 & -2 & -3 & 3 & 4 & -5 & 20 & 2 & -8 & 2 \\ 36 & 70 & 15 & 6 & 0 & 5 & 6 & -6 & -24 & -5 & 1 & 8 & -2 & 0 \\ -5 & 15 & 80 & -1 & 0 & -4 & 6 & 4 & 72 & 7 & -1 & 1 & 1 & -5 \\ -3 & 6 & -1 & 140 & 4 & 71 & 24 & -4 & -2 & 0 & -3 & 3 & 2 & -3 \\ 1 & 0 & 0 & 4 & 775 & 9 & -4 & -4 & 0 & 1 & 1 & -2 & -1 & 0 \\ -2 & 5 & -4 & 71 & 9 & 615 & 16 & -5 & 2 & 0 & -2 & 2 & 2 & -2 \\ -3 & 6 & 6 & 24 & -4 & 16 & 525 & -4 & -5 & 1 & -2 & 3 & 3 & -3 \\ 3 & -6 & 4 & -4 & -4 & -5 & -4 & 395 & 24 & 43 & 5 & -1 & -2 & 1 \\ 4 & -24 & 72 & -2 & 0 & 2 & -5 & 24 & 855 & -2 & 4 & -1 & -2 & 2 \\ -5 & -5 & 7 & 0 & 1 & 0 & 1 & 43 & -2 & 0 & -26 & 13 & 6 & -1 \\ 20 & 1 & -1 & -3 & 1 & -2 & -2 & 5 & 4 & -26 & 150 & 99 & -3 & 1 \\ 2 & 8 & 1 & 3 & -2 & 2 & 3 & -1 & -1 & 13 & 99 & 180 & 0 & 0 \\ -8 & -2 & 1 & 2 & -1 & 2 & 3 & -2 & -2 & 6 & -3 & 0 & 90 & -36 \\ 2 & 0 & -5 & -3 & 0 & -2 & -3 & 1 & 2 & -1 & 1 & 0 & -36 & 200 \end{pmatrix} \text{cm}^{-1} \quad (D1)$$



for model 1, and

$$\mathbf{H}_{\text{LE},s} = (E_{\text{LE}} + \lambda_{\text{D,Chl}^*})\mathbf{1} + \begin{pmatrix} 816.00 & 49.64 & -5.89 & -2.51 & 0.77 & -1.87 & -2.49 & 2.78 & 3.79 & -5.95 & 24.89 & 9.13 & -10.79 & 3.59 \\ 49.64 & 84.00 & 38.11 & 6.42 & -0.71 & 5.60 & 7.13 & -5.84 & -19.25 & -11.39 & 9.69 & 15.83 & -4.96 & 0.69 \\ -5.89 & 38.11 & 214.00 & -3.28 & 1.13 & -8.89 & 1.23 & 6.72 & 96.66 & 12.97 & -2.70 & -0.76 & 2.68 & -6.70 \\ -2.51 & 6.42 & -3.28 & 387.00 & 3.35 & 104.56 & 35.93 & -2.76 & -7.28 & -4.18 & -3.80 & 4.67 & 2.12 & -3.42 \\ 0.77 & -0.71 & 1.13 & 3.35 & 606.00 & 29.71 & -4.47 & -5.13 & -0.77 & 1.61 & 1.33 & -2.85 & -1.40 & 0.37 \\ -1.87 & 5.60 & -8.89 & 104.56 & 29.71 & 777.00 & 59.38 & -4.99 & -0.16 & -3.28 & -2.52 & 3.10 & 1.47 & -2.16 \\ -2.49 & 7.13 & 1.23 & 35.93 & -4.47 & 59.38 & 641.00 & -4.43 & -11.99 & -0.14 & -2.78 & 3.07 & 2.20 & -3.25 \\ 2.78 & -5.84 & 6.72 & -2.76 & -5.13 & -4.99 & -4.43 & 688.00 & 36.07 & 61.97 & 4.35 & -1.08 & -2.01 & 1.30 \\ 3.79 & -19.25 & 96.66 & -7.28 & -0.77 & -0.16 & -11.99 & 36.07 & 648.00 & 3.86 & 4.30 & -2.57 & -2.92 & 2.33 \\ -5.95 & -11.39 & 12.97 & -4.18 & 1.61 & -3.28 & -0.14 & 61.97 & 3.86 & 0.00 & -24.96 & 23.10 & 7.21 & -1.55 \\ 24.89 & 9.69 & -2.70 & -3.80 & 1.33 & -2.52 & -2.78 & 4.35 & 4.30 & -24.96 & 39.00 & 126.92 & -6.15 & 4.55 \\ 9.13 & 15.83 & -0.76 & 4.67 & -2.85 & 3.10 & 3.07 & -1.08 & -2.57 & 23.10 & 126.92 & 21.00 & -0.47 & -0.18 \\ -10.79 & -4.96 & 2.68 & 2.12 & -1.40 & 1.47 & 2.20 & -2.01 & -2.92 & 7.21 & -6.15 & -0.47 & 101.00 & -50.22 \\ 3.59 & 0.69 & -6.70 & -3.42 & 0.37 & -2.16 & -3.25 & 1.30 & 2.33 & -1.55 & 4.55 & -0.18 & -50.22 & 187.00 \end{pmatrix} \text{cm}^{-1} \quad (\text{D2})$$

for model 2. The columns/rows correspond to the states in the following order:  $b601^*$ ,  $a602^*$ ,  $a603^*$ ,  $a604^*$ ,  $b605^*$ ,  $b606^*$ ,  $b607^*$ ,  $b608^*$ ,  $b609^*$ ,  $a610^*$ ,  $a611^*$ ,  $a612^*$ ,  $a613^*$ ,  $a614^*$ . In these Hamiltonians we incorporate the reorganization energy contribution of the LE baths into the system Hamiltonian matrices, and as such diagonal elements correspond to vertical excitation energies in the absence of LE coupling, and the diagonal element minus  $\lambda_{\text{D,Chl}^*}$  is the free energy of that LE state in the absence of inter LE state coupling. The CT state system Hamiltonians are given by

$$\hat{H}_{\text{CT}_1,s} = (E_{a612^*} + \Delta G_{\text{CT}_1}) |\text{CT}_1\rangle\langle\text{CT}_1| \quad (\text{D3})$$

$$\hat{H}_{\text{CT}_2,s} = (E_{a603^*} + \Delta G_{\text{CT}_2}) |\text{CT}_2\rangle\langle\text{CT}_2| \quad (\text{D4})$$

where  $E_{a612^*}$  and  $E_{a603^*}$  are the diagonal elements of  $\mathbf{H}_{\text{LE},s}$  corresponding to the states  $a612^*$  and  $a603^*$  respectively. Here  $\text{CT}_1$  is the  $a612^-\text{Lut}1^+$  state and  $\text{CT}_2$  is the  $a603^-\text{Lut}2^+$  state. Finally  $\hat{H}_{\text{GS},s} = 0$  by definition. The remaining model parameters are listed in Tab. I.

The  $G_{AB}^B(t)$  and  $G_{BA}^B(t)$  functions were evaluated using<sup>51,53</sup>

$$G_{AB}^B(t) = G_{BA}^B(t)^* = \exp(\zeta_{AB}(t) + i\Delta\epsilon_{AB}t/\hbar) \quad (\text{D5})$$

$$\zeta_{AB}(t) = - \int_0^\infty d\omega \frac{\mathcal{J}_{AB}(\omega)}{\omega^2} \times \left[ \coth\left(\frac{\beta\hbar\omega}{2}\right) (1 - \cos(\omega t)) + i \sin(\omega t) \right] \quad (\text{D6})$$

where  $\mathcal{J}_{AB}(\omega)$  is the  $b_{\text{CT}}$  spectral density associated with the  $A \rightarrow B$  charge transfer, and  $\Delta\epsilon_{AB}$  is the free energy change excluding  $b_{\text{LE}}$  contributions (i.e. the free energy change with  $\hat{B}_{n,r} = 0$ ). In order to evaluate the integrals over these functions, each component of the spectral density (the Debye and Brownian Oscillator components) was discretized into 512 frequencies using a Gauss-Legendre quadrature for the function  $(1/(4\pi\lambda))\mathcal{J}_{\text{D/BO}}(\omega)/\omega$ ,<sup>89</sup> and using this the  $\zeta_{AB}(t)$  function was evaluated and the required numerical integrals were evaluated using the trapezium rule. The integrals were evaluated

up to  $t_{\text{max}} = 23.5$  fs, discretized into 1000 time points for the CT-LE correlation functions and 14104 time points for the much more oscillatory CT-GS correlation functions. The same expressions and methodology were used to evaluate the ET kernel for the dimer model in Sec. IV.

## REFERENCES

<sup>1</sup>T. Mirkovic, E. E. Ostroumov, J. M. Anna, R. van Grondelle, Govindjee, and G. D. Scholes, "Light Absorption and Energy Transfer in the Antenna Complexes of Photosynthetic Organisms," *Chem. Rev.* **117**, 249–293 (2017).

| Parameter                  | Value (cm <sup>-1</sup> unless specified otherwise) |
|----------------------------|---|
| $\Delta G_{\text{CT}_1}$   | -82   |
| $\lambda_{\text{CT}_1}$    | 5405  |
| $V_{\text{CT}_1}$          | 240   |
| $\Delta G_{\text{CT}_2}$   | 951   |
| $\lambda_{\text{CT}_2}$    | 5052  |
| $V_{\text{CT}_2}$          | 279   |
| $\omega_{\text{D,CT}}$     | 30  |
| $\Omega$                   | 1500  |
| $\gamma$                   | 50  |
| $E_{\text{LE}}$ (Model 1)  | 14780   |
| $E_{\text{LE}}$ (Model 2)  | 15073   |
| $\lambda_{\text{D,Chl}^*}$ | 220   |
| $\omega_{\text{D,Chl}^*}$  | 353.6777  |
| $\mu_{\text{Chl}a}$        | 4.0 D   |
| $\mu_{\text{Chl}b}$        | 3.4 D   |
| $k_{\text{NR}}$            | 0.25 ns <sup>-1</sup>                               |

TABLE I. Parameters used for the LHCI monomer CT quenching models.

- <sup>2</sup>D. J. Vinyard, G. M. Ananyev, and G. Charles Dismukes, "Photosystem II: The Reaction Center of Oxygenic Photosynthesis," *Annu. Rev. Biochem.* **82**, 577–606 (2013).
- <sup>3</sup>M. Gorka, A. Baldansuren, A. Malnati, E. Gruszecki, J. H. Golbeck, and K. V. Lakshmi, "Shedding Light on Primary Donors in Photosynthetic Reaction Centers," *Front. Microbiol.* **12**, 1–31 (2021).
- <sup>4</sup>R. E. Blankenship, ed., *Molecular Mechanisms of Photosynthesis* (Blackwell Science Ltd, Oxford, UK, 2002).
- <sup>5</sup>R. Croce and H. van Amerongen, "Light-harvesting and structural organization of Photosystem II: From individual complexes to thylakoid membrane," *J. Photochem. Photobiol. B Biol.* **104**, 142–153 (2011).
- <sup>6</sup>R. Goss and B. Lepetit, "Biodiversity of NPQ," *J. Plant Physiol.* **172**, 13–32 (2015).
- <sup>7</sup>S. Park, C. J. Steen, D. Lyska, A. L. Fischer, B. Endelman, M. Iwai, K. K. Niyogi, and G. R. Fleming, "Chlorophyll–carotenoid excitation energy transfer and charge transfer in *Nannochloropsis oceanica* for the regulation of photosynthesis," *Proc. Natl. Acad. Sci.* **116**, 3385–3390 (2019).
- <sup>8</sup>A. V. Ruban and F. Saccon, "Chlorophyll a de-excitation pathways in the LHClI antenna," *J. Chem. Phys.* **156**, 070902 (2022).
- <sup>9</sup>A. Pinnola, H. Staleva-Musto, S. Capaldi, M. Ballottari, R. Bassi, and T. Polívka, "Electron transfer between carotenoid and chlorophyll contributes to quenching in the LHCSR1 protein from *Physcomitrella patens*," *Biochim. Biophys. Acta - Bioenerg.* **1857**, 1870–1878 (2016).
- <sup>10</sup>E. E. Ostroumov, J. P. Götz, M. Reus, P. H. Lambrev, and A. R. Holzwarth, "Characterization of fluorescent chlorophyll charge-transfer states as intermediates in the excited state quenching of light-harvesting complex II," *Photosynth. Res.* **144**, 171–193 (2020).
- <sup>11</sup>Y. Tanimura and R. Kubo, "Time Evolution of a Quantum System in Contact with a Nearly Gaussian-Markoffian Noise Bath," *J. Phys. Soc. Japan* **58**, 101–114 (1989).
- <sup>12</sup>A. Ishizaki and G. R. Fleming, "Theoretical examination of quantum coherence in a photosynthetic system at physiological temperature," *Proc. Natl. Acad. Sci.* **106**, 17255–17260 (2009).
- <sup>13</sup>Y. Tanimura, "Numerically "exact" approach to open quantum dynamics: The hierarchical equations of motion (HEOM)," *J. Chem. Phys.* **153**, 020901 (2020).
- <sup>14</sup>A. Ishizaki and G. R. Fleming, "Unified treatment of quantum coherent and incoherent hopping dynamics in electronic energy transfer: Reduced hierarchy equation approach," *J. Chem. Phys.* **130**, 234111 (2009).
- <sup>15</sup>M. Sarovar, A. Ishizaki, G. R. Fleming, and K. B. Whaley, "Quantum entanglement in photosynthetic light-harvesting complexes," *Nat. Phys.* **6**, 462–467 (2010), arXiv:0905.3787.
- <sup>16</sup>J. Strümpfer and K. Schulten, "Light harvesting complex II B850 excitation dynamics," *J. Chem. Phys.* **131**, 225101 (2009).
- <sup>17</sup>A. Ishizaki, T. R. Calhoun, G. S. Schlau-Cohen, and G. R. Fleming, "Quantum coherence and its interplay with protein environments in photosynthetic electronic energy transfer," *Phys. Chem. Chem. Phys.* **12**, 7319 (2010).
- <sup>18</sup>L. Chen, R. Zheng, Y. Jing, and Q. Shi, "Simulation of the two-dimensional electronic spectra of the Fenna-Matthews-Olson complex using the hierarchical equations of motion method," *J. Chem. Phys.* **134**, 194508 (2011).
- <sup>19</sup>C. Kreisbeck, T. Kramer, M. Rodríguez, and B. Hein, "High-Performance Solution of Hierarchical Equations of Motion for Studying Energy Transfer in Light-Harvesting Complexes," *J. Chem. Theory Comput.* **7**, 2166–2174 (2011).
- <sup>20</sup>A. G. Dijkstra and Y. Tanimura, "The role of the environment time scale in light-harvesting efficiency and coherent oscillations," *New J. Phys.* **14**, 073027 (2012).
- <sup>21</sup>C. Kreisbeck, T. Kramer, and A. Aspuru-Guzik, "Scalable High-Performance Algorithm for the Simulation of Exciton Dynamics. Application to the Light-Harvesting Complex II in the Presence of Resonant Vibrational Modes," *J. Chem. Theory Comput.* **10**, 4045–4054 (2014).
- <sup>22</sup>M. Schröter, T. Pullerits, and O. Kühn, "Unraveling the quantum state mixing of excitonic and vibronic excitations in the dynamics of molecular aggregates," *Ann. Phys.* **527**, 536–545 (2015).
- <sup>23</sup>H. C. H. Chan, O. E. Gamel, G. R. Fleming, and K. B. Whaley, "Single-photon absorption by single photosynthetic light-harvesting complexes," *J. Phys. B At. Mol. Opt. Phys.* **51**, 054002 (2018), arXiv:1801.04924.
- <sup>24</sup>V. Janković and T. Mančal, "Exact description of excitonic dynamics in molecular aggregates weakly driven by light," *J. Chem. Phys.* **153**, 244122 (2020), arXiv:2001.07180.
- <sup>25</sup>Y. Yan, Y. Liu, T. Xing, and Q. Shi, "Theoretical study of excitation energy transfer and nonlinear spectroscopy of photosynthetic light-harvesting complexes using the nonperturbative reduced dynamics method," *WIREs Comput. Mol. Sci.* **11**, 1–25 (2021).
- <sup>26</sup>V. I. Novoderezhkin, R. Croce, M. Wahadoszamen, I. Polukhina, E. Romero, and R. van Grondelle, "Mixing of exciton and charge-transfer states in light-harvesting complex Lhca4," *Phys. Chem. Chem. Phys.* **18**, 19368–19377 (2016).
- <sup>27</sup>J. Blumberger, "Recent Advances in the Theory and Molecular Simulation of Biological Electron Transfer Reactions," *Chem. Rev.* **115**, 11191–11238 (2015).
- <sup>28</sup>Q. Shi, L. Chen, G. Nan, R.-X. Xu, and Y. Yan, "Efficient hierarchical Liouville space propagator to quantum dissipative dynamics," *J. Chem. Phys.* **130**, 084105 (2009).
- <sup>29</sup>Q. Shi, L. Chen, G. Nan, R. Xu, and Y. Yan, "Electron transfer dynamics: Zusman equation versus exact theory," *J. Chem. Phys.* **130**, 164518 (2009).
- <sup>30</sup>T. Firmino, E. Mangaud, F. Cailliez, A. Devolder, D. Mendive-Tapia, F. Gatti, C. Meier, M. Desouter-Lecomte, and A. de la Lande, "Quantum effects in ultrafast electron transfers within cryptochromes," *Phys. Chem. Chem. Phys.* **18**, 21442–21457 (2016).
- <sup>31</sup>Q. Shi, Y. Xu, Y. Yan, and M. Xu, "Efficient propagation of the hierarchical equations of motion using the matrix product state method," *J. Chem. Phys.* **148**, 174102 (2018).
- <sup>32</sup>R. Borrelli, "Density matrix dynamics in twin-formulation: An efficient methodology based on tensor-train representation of reduced equations of motion," *J. Chem. Phys.* **150**, 234102 (2019).
- <sup>33</sup>Y. Ke, R. Borrelli, and M. Thoss, "Hierarchical equations of motion approach to hybrid fermionic and bosonic environments: Matrix product state formulation in twin space," *J. Chem. Phys.* **156**, 194102 (2022), arXiv:2202.10273.
- <sup>34</sup>Y. Yan, M. Xu, T. Li, and Q. Shi, "Efficient propagation of the hierarchical equations of motion using the Tucker and hierarchical Tucker tensors," *J. Chem. Phys.* **154**, 194104 (2021).
- <sup>35</sup>L. P. Lindoy, *PhD thesis*, Phd thesis, University of Oxford (2019).
- <sup>36</sup>M. Richter and B. P. Fingerhut, "Electron Transfer Pathways and Dynamics in *Drosophila* Cryptochrome - the Role of Protein Electrostatics," *EPJ Web Conf.* **205**, 10009 (2019).
- <sup>37</sup>M. Richter and B. P. Fingerhut, "Coupled excitation energy and charge transfer dynamics in reaction centre inspired model systems," *Faraday Discuss.* **216**, 72–93 (2019).
- <sup>38</sup>W. M. Zhang, T. Meier, V. Chernyak, and S. Mukamel, "Exciton-migration and three-pulse femtosecond optical spectroscopies of photosynthetic antenna complexes," *J. Chem. Phys.* **108**, 7763–7774 (1998).
- <sup>39</sup>G. D. Scholes and G. R. Fleming, "On the Mechanism of Light Harvesting in Photosynthetic Purple Bacteria: B800 to B850 Energy Transfer," *J. Phys. Chem. B* **104**, 1854–1868 (2000).
- <sup>40</sup>V. I. Novoderezhkin and R. van Grondelle, "Physical origins and models of energy transfer in photosynthetic light-harvesting," *Phys. Chem. Chem. Phys.* **12**, 7352 (2010).
- <sup>41</sup>V. Novoderezhkin, A. Marin, and R. van Grondelle, "Intra- and inter-monomeric transfers in the light harvesting LHClI complex: the Redfield–Förster picture," *Phys. Chem. Chem. Phys.* **13**, 17093 (2011).
- <sup>42</sup>V. I. Novoderezhkin, R. Croce, and R. van Grondelle, "Dynamics of the mixed exciton and charge-transfer states in light-harvesting complex Lhca4: Hierarchical equation approach," *Biochim. Biophys. Acta - Bioenerg.* **1859**, 655–665 (2018).
- <sup>43</sup>A. Kelly and Y. M. Rhee, "Mixed Quantum-Classical Description of Excitation Energy Transfer in a Model Fenna-Matthews-Olson Complex," *J. Phys. Chem. Lett.* **2**, 808–812 (2011).
- <sup>44</sup>P. Huo and D. F. Coker, "Communication: Partial linearized density matrix dynamics for dissipative, non-adiabatic quantum evolution," *J. Chem. Phys.* **135**, 201101 (2011).
- <sup>45</sup>H. W. Kim, A. Kelly, J. W. Park, and Y. M. Rhee, "All-Atom Semiclassical Dynamics Study of Quantum Coherence in Photosynthetic Fenna–Matthews–Olson Complex," *J. Am. Chem. Soc.* **134**, 11640–11651 (2012).
- <sup>46</sup>W. C. Pfalzgraff, A. Montoya-Castillo, A. Kelly, and T. E. Markland, "Efficient construction of generalized master equation memory kernels for multi-state systems from nonadiabatic quantum-classical dynamics," *J. Chem. Phys.* **150**, 244109 (2019), arXiv:1903.09608.

- <sup>47</sup>J. E. Runeson and J. O. Richardson, "Generalized spin mapping for quantum-classical dynamics," *J. Chem. Phys.* **152**, 084110 (2020), arXiv:1912.10906.
- <sup>48</sup>J. R. Mannouch and J. O. Richardson, "A partially linearized spin-mapping approach for nonadiabatic dynamics. I. Derivation of the theory," *J. Chem. Phys.* **153**, 194109 (2020), arXiv:2007.05047.
- <sup>49</sup>J. E. Runeson, J. E. Lawrence, J. R. Mannouch, and J. O. Richardson, "Explaining the Efficiency of Photosynthesis: Quantum Uncertainty or Classical Vibrations?" *J. Phys. Chem. Lett.* **13**, 3392–3399 (2022).
- <sup>50</sup>M. Sparpaglione and S. Mukamel, "Dielectric friction and the transition from adiabatic to nonadiabatic electron transfer. I. Solvation dynamics in Liouville space," *J. Chem. Phys.* **88**, 3263–3280 (1988).
- <sup>51</sup>T. P. Fay, L. P. Lindoy, and D. E. Manolopoulos, "Spin-selective electron transfer reactions of radical pairs: Beyond the Haberkorn master equation," *J. Chem. Phys.* **149**, 064107 (2018), arXiv:1808.03211.
- <sup>52</sup>T. P. Fay, "Chirality-Induced Spin Coherence in Electron Transfer Reactions," *J. Phys. Chem. Lett.* **12**, 1407–1412 (2021), arXiv:2101.03104.
- <sup>53</sup>T. P. Fay and D. T. Limmer, "Origin of Chirality Induced Spin Selectivity in Photoinduced Electron Transfer," *Nano Lett.* **21**, 6696–6702 (2021), arXiv:2106.06554.
- <sup>54</sup>M. Thoss, H. Wang, and W. H. Miller, "Self-consistent hybrid approach for complex systems: Application to the spin-boson model with debye spectral density," *The Journal of Chemical Physics* **115**, 2991–3005 (2001).
- <sup>55</sup>T. C. Berkelbach, D. R. Reichman, and T. E. Markland, "Reduced density matrix hybrid approach: An efficient and accurate method for adiabatic and non-adiabatic quantum dynamics," *The Journal of Chemical Physics* **136**, 034113 (2012).
- <sup>56</sup>A. Montoya-Castillo, T. C. Berkelbach, and D. R. Reichman, "Extending the applicability of redfield theories into highly non-markovian regimes," *The Journal of Chemical Physics* **143**, 194108 (2015).
- <sup>57</sup>A. J. Schile and D. T. Limmer, "Simulating conical intersection dynamics in the condensed phase with hybrid quantum master equations," *The Journal of Chemical Physics* **151**, 014106 (2019).
- <sup>58</sup>S. Nakajima, "On Quantum Theory of Transport Phenomena," *Prog. Theor. Phys.* **20**, 948–959 (1958).
- <sup>59</sup>R. Zwanzig, "Ensemble method in the theory of irreversibility," *J. Chem. Phys.* **33**, 1338–1341 (1960).
- <sup>60</sup>H. Mori, "Transport, Collective Motion, and Brownian Motion," *Prog. Theor. Phys.* **33**, 423–455 (1965).
- <sup>61</sup>F. Müh, M. E. A. Madjet, and T. Renger, "Structure-based identification of energy sinks in plant light-harvesting complex II," *J. Phys. Chem. B* **114**, 13517–13535 (2010).
- <sup>62</sup>L. Cupellini, D. Calvani, D. Jacquemin, and B. Mennucci, "Charge transfer from the carotenoid can quench chlorophyll excitation in antenna complexes of plants," *Nat. Commun.* **11**, 662 (2020).
- <sup>63</sup>Z. Liu, H. Yan, K. Wang, T. Kuang, J. Zhang, L. Gui, X. An, and W. Chang, "Crystal structure of spinach major light-harvesting complex at 2.72 Å resolution," *Nature* **428**, 287–292 (2004).
- <sup>64</sup>R. Bennett, T. M. Barlow, and A. Beige, "A physically motivated quantization of the electromagnetic field," *Eur. J. Phys.* **37**, 014001 (2016), arXiv:1506.03305.
- <sup>65</sup>M. K. Lee and D. F. Coker, "Modeling Electronic-Nuclear Interactions for Excitation Energy Transfer Processes in Light-Harvesting Complexes," *J. Phys. Chem. Lett.* **7**, 3171–3178 (2016).
- <sup>66</sup>J. Segarra-Martí, F. Segatta, T. A. Mackenzie, A. Nenov, I. Rivalta, M. J. Bearpark, and M. Garavelli, "Modeling multidimensional spectral line-shapes from first principles: application to water-solvated adenine," *Faraday Discuss.* **221**, 219–244 (2020).
- <sup>67</sup>T. J. Zuehlsdorff, S. V. Shedge, S.-Y. Lu, H. Hong, V. P. Aguirre, L. Shi, and C. M. Isborn, "Vibronic and Environmental Effects in Simulations of Optical Spectroscopy," *Annu. Rev. Phys. Chem.* **72**, 165–188 (2021).
- <sup>68</sup>A. Ishizaki and Y. Tanimura, "Quantum dynamics of system strongly coupled to low-temperature colored noise bath: Reduced hierarchy equations approach," *J. Phys. Soc. Japan* **74**, 3131–3134 (2005).
- <sup>69</sup>T. Ikeda and A. Nakayama, "Collective bath coordinate mapping of "hierarchy" in hierarchical equations of motion," *J. Chem. Phys.* **156**, 104104 (2022), arXiv:2112.09861.
- <sup>70</sup>L. Ko, R. L. Cook, and K. B. Whaley, "Dynamics of photosynthetic light harvesting systems interacting with N-photon Fock states," *J. Chem. Phys.* **156**, 244108 (2022), arXiv:2111.06996.
- <sup>71</sup>R. A. Marcus, "On the theory of oxidation-reduction reactions involving electron transfer. I," *J. Chem. Phys.* **24**, 966–978 (1956).
- <sup>72</sup>N. S. Hush, "Adiabatic rate processes at electrodes. I. Energy-charge relationships," *J. Chem. Phys.* **28**, 962–972 (1958).
- <sup>73</sup>T. P. Fay, "A simple improved low temperature correction for the hierarchical equations of motion," *J. Chem. Phys.* **014101** (2022), 10.1063/5.0100365, arXiv:2205.09270.
- <sup>74</sup>A. V. Ruban and S. Wilson, "The Mechanism of Non-Photochemical Quenching in Plants: Localization and Driving Forces," *Plant Cell Physiol.* **62**, 1063–1072 (2021).
- <sup>75</sup>D. I. Bennett, K. Amarnath, and G. R. Fleming, "A structure-based model of energy transfer reveals the principles of light harvesting in photosystem II supercomplexes," *J. Am. Chem. Soc.* **135**, 9164–9173 (2013).
- <sup>76</sup>S. Bourne Worster, C. Stross, F. M. W. C. Vaughan, N. Linden, and F. R. Manby, "Structure and Efficiency in Bacterial Photosynthetic Light Harvesting," *J. Phys. Chem. Lett.* **10**, 7383–7390 (2019), arXiv:1908.08373.
- <sup>77</sup>T. P. Fay, "heom-lab: A Matlab code for performing HEOM calculations," <https://github.com/tomfay/heom-lab> (2022).
- <sup>78</sup>V. Balevičius, K. F. Fox, W. P. Bricker, S. Jurinovich, I. G. Prandi, B. Mennucci, and C. D. P. Duffy, "Fine control of chlorophyll-carotenoid interactions defines the functionality of light-harvesting proteins in plants," *Sci. Rep.* **7**, 13956 (2017).
- <sup>79</sup>A. H. Short, T. P. Fay, T. Crisanto, J. Hall, C. J. Steen, K. K. Niyogi, D. T. Limmer, and G. R. Fleming, "Xanthophyll-cycle based model of the rapid photoprotection of Nannochloropsis in response to regular and irregular light/dark sequences," *J. Chem. Phys.* **156**, 205102 (2022).
- <sup>80</sup>A. Chrysafoudi, S. Maity, U. Kleinekathöfer, and V. Daskalakis, "Robust Strategy for Photoprotection in the Light-Harvesting Antenna of Diatoms: A Molecular Dynamics Study," *J. Phys. Chem. Lett.* **12**, 9626–9633 (2021).
- <sup>81</sup>V. Daskalakis, S. Papadatos, and T. Stergiannakos, "The conformational phase space of the photoprotective switch in the major light harvesting complex II," *Chem. Commun.* **56**, 11215–11218 (2020).
- <sup>82</sup>M. Lapillo, E. Cignoni, L. Cupellini, and B. Mennucci, "The energy transfer model of nonphotochemical quenching: Lessons from the minor CP29 antenna complex of plants," *Biochim. Biophys. Acta - Bioenerg.* **1861**, 148282 (2020).
- <sup>83</sup>S. Maity, V. Daskalakis, M. Elstner, and U. Kleinekathöfer, "Multiscale QM/MM molecular dynamics simulations of the trimeric major light-harvesting complex II," *Phys. Chem. Chem. Phys.* **23**, 7407–7417 (2021).
- <sup>84</sup>J. E. Lawrence and D. E. Manolopoulos, "Path integral methods for reaction rates in complex systems," *Faraday Discuss.* **221**, 9–29 (2020).
- <sup>85</sup>E. Rabani, S. A. Egorov, and B. J. Berne, "Classical Approximation to Nonradiative Electronic Relaxation in Condensed Phase Systems," *J. Phys. Chem. A* **103**, 9539–9544 (1999).
- <sup>86</sup>S. A. Egorov, E. Rabani, and B. J. Berne, "On the Adequacy of Mixed Quantum-Classical Dynamics in Condensed Phase Systems," *J. Phys. Chem. B* **103**, 10978–10991 (1999).
- <sup>87</sup>Z. Tong, X. Gao, M. S. Cheung, B. D. Dunietz, E. Geva, and X. Sun, "Charge transfer rate constants for the carotenoid-porphyrin-C 60 molecular triad dissolved in tetrahydrofuran: The spin-boson model vs the linearized semiclassical approximation," *J. Chem. Phys.* **153**, 044105 (2020).
- <sup>88</sup>J. E. Lawrence and D. E. Manolopoulos, "Analytic continuation of Wolynes theory into the Marcus inverted regime," *J. Chem. Phys.* **148**, 102313 (2018), arXiv:1710.11113.
- <sup>89</sup>J. E. Lawrence and D. E. Manolopoulos, "An improved path-integral method for golden-rule rates," *J. Chem. Phys.* **153**, 154113 (2020).
- <sup>90</sup>E. Cignoni, V. Slama, L. Cupellini, and B. Mennucci, "The atomistic modeling of light-harvesting complexes from the physical models to the computational protocol," *J. Chem. Phys.* **156**, 120901 (2022).